REVIEW ARTICLE

X-ray telescopes

Rep. Prog. Phys., vol 48, pp 579-629, 1985. Printed in Great Britain

X-ray telescopes

B Aschenbach

Max-Planck-Institut für Physik und Astrophysik, Institut für Extraterrestrische Physik,
8046 Garching bei München, West Germany

Abstract

This review summarises the present knowledge about x-ray reflection from real mirrors, with particular emphasis on x-ray scattering. The mirror configurations for a telescope are presented and their imaging capabilities are discussed. The fabrication techniques and the supporting metrology methods used for the manufacture of highly aspherical telescope mirrors are outlined, including direct grinding and polishing as well as replication methods. An account is given of the achievements obtained so far for the telescopes built for solar and non-solar x-ray astronomy applications.

This review was received in October 1984.

0034-4885/85/050579+51$09.00

Contents

1. Introduction

In 1895 Röntgen reported his discovery of x-rays, and in 1912 von Laue demonstrated with his famous experiments that x-rays are diffracted when passing through a crystal. It took another decade of research before Compton showed in 1923 that x-rays can be reflected from a polished surface. In recognition of the fact that the angle of incidence was so small with respect to the plane of the surface ($\leqslant 1°$) the term 'glancing' or 'grazing incidence reflection' was born. Obviously, total external reflection occurred which meant that the interaction of x-rays with matter could be described by an index of refraction which was less than unity. These discoveries established the electromagnetic wave character of x-rays and opened up the new research field of x-ray imaging optics. The most appealing application at the time was the possibility of constructing an x-ray microscope which could, in principle, operate with a much greater resolving power than an ordinary optical microscope. An overview of the problems related to constructing real imaging x-ray mirrors was presented by Jentzsch in 1929. He extensively discussed mirror geometries required to focus x-rays, and concluded that it was impossible to form good images by means of a single spherical mirror because of the extreme astigmatism resulting from the grazing incidence condition. This difficulty could, however, be overcome by a single mirror surface with two very different radii of curvature and he proposed the use of toroidal mirrors. He also recommended the use of cylindrical mirrors and the improvements were described which could be obtained by using two mirrors at successive reflections.

Although the basic ideas for x-ray imaging had been laid down in this early work it was much later, in 1948, when the first two-dimensional x-ray image was obtained by Kirkpatrick and Baez. They used two orthogonally crossed cylindrical mirrors, each of which provided one-dimensional focusing. Ehrenberg (1949a) successfully produced a line image of a fine slit with an optical flat which was mechanically bent into an elliptical cylinder. He also noticed x-ray stray light outside the focus which he attributed to physical imperfections of the polished mirror surface. In an accompanying paper (1949b) he suggested that these surface irregularities left over from the polishing process could be described by a Fourier series. Thus, at a given Fourier component the x-rays are diffracted so that, besides the zero-order image, two first-order images appear, their angular distance from the focus being inversely proportional to the spatial wavelength and their intensity being proportional to the square of the amplitude. By contaminating mirror surfaces of good optical quality with sinusoidally shaped gold strips he was able to verify this by measurement. He demonstrated that mirror surfaces have to be polished to an extremely low level of surface roughness in order to provide a decent image. At a grazing angle of 2°, a surface roughness with a height of about the x-ray wavelength used will scatter 20% of the total reflected x-rays off the image focus.

Thus, at the beginning of the 1950s there were two major difficulties in constructing useful x-ray imaging systems: (i) a mirror configuration was still lacking which could overcome the deficiencies of the Kirkpatrick–Baez solution, i.e. small aperture, low resolution and geometric aberrations; (ii) the appropriate technology had to be developed which allows x-ray mirrors to be figured and polished to the required surface

accuracy. The latter is, of course, possible in a controlled and repeatable manner only if the corresponding metrology is available.

The first problem was solved by Wolter in 1951. He analysed mirrors which have concentric figures of revolution, i.e. paraboloids, hyperboloids and ellipsoids. He showed that in order to achieve a true image over an extended field of view the x-rays have to undergo two successive reflections from either a paraboloid/hyperboloid or paraboloid/ellipsoid combination which are mounted in a coaxial and confocal arrangement. Wolter himself discussed this type of optics in the context of microscopes. Hence the primary goal of these investigations was to achieve optics with the potential of high resolution. However, it became evident rather soon that the problems related to the fabrication of these highly aspherical mirrors were severe and the prospects for making substantial progress were not too good. This problem, the second one, was eventually attacked and solved in the context of building telescopes for x-ray astronomy.

In 1948 Burnight discovered that the Sun emitted x-rays, and his results from exposing casettes of photographic film at the top of the Earth's atmosphere on a V2 rocket flight ushered in the era of solar x-ray research. The first x-ray picture of the Sun was obtained in 1960 with a pinhole camera experiment, again on a sounding rocket flight (Chubb *et al* 1961). In 1960 Giacconi and Rossi pointed out that future x-ray astronomy would greatly benefit from the use of focusing optics because of their increased collecting area and angular resolution and thus greatly improved signal-to-noise ratio. Originally proposing a paraboloid they extended their idea to include the true imaging devices of the Wolter type. This was the first time that grazing incidence optics were suggested as a method of constructing an x-ray telescope. In 1961 the first x-ray collector of about 1 cm^2 collecting area was completed: a glass cone with the interior surface optically polished (Giacconi *et al* 1981). The first flight of a Wolter-type telescope occurred on a sounding rocket on 15 October 1963, and the first x-ray pictures of the Sun taken by a grazing incidence telescope were recorded on film. The telescope was not made from glass but of electroformed nickel and its angular resolution was better than 1 arcmin (Giacconi *et al* 1981). In the ten years that followed the techniques of the mirror production advanced and reached a peak in the S-054 and S-056 telescopes which provided a couple of arcsecond resolution. These instruments were part of the Apollo Telescope Mount flown on Skylab in 1973.

In 1962 the first non-solar celestial x-ray source was discovered with a Geiger counter on a sounding rocket flight (Giacconi *et al* 1962). Non-solar x-ray astronomy became a reality and, as in solar research, imaging telescopes would have been well suited to advance the field. But until the end of the 1970s only a few grazing incidence telescopes of the Wolter and Kirkpatrick–Baez type with more or less good angular resolutions were built and flown on sounding rockets. The first imaging x-ray telescope to orbit the Earth on a satellite was launched in November 1978 and was in operation until April 1981. It was carried on the second of the series of three High Energy Astronomy Observatory Satellites (HEAO-B) of the United States of America and was renamed the Einstein observatory after launch. The Einstein telescope represented an extraordinary step forward in the development of grazing incidence imaging systems with respect to collecting area and angular resolution. Due to the tremendous improvement of signal-to-noise ratio compared with collimated counter devices used earlier the Einstein telescope detected x-rays from almost all classes of known astronomical objects, encompassing nearby normal stars to quasars at cosmological distances.

The sequence of successful x-ray telescopes in orbit continued with the European Exosat satellite which was launched in May 1983. In addition to a proportional counter

array and a gas scintillation proportional counter it carried two Wolter-type x-ray telescopes which are smaller in size and of lower angular resolution than the Einstein optics. The Einstein, as well as the Exosat, telescopes were operated in a pointing mode, switching from target to target which had been pre-selected from the ground, covering only a small fraction of the sky in total. In contrast to this concept the primary scientific objective of the German Rosat (Röntgensatellit) mission is to perform the first all-sky survey by means of an x-ray imaging telescope, whose largest mirror has a diameter of 83 cm. After completion of the survey detailed observations of selected sources with respect to spatial structures, spectra and time variability will be made in pointing mode. Rosat will be launched in the second half of 1987. The grazing incidence mirror system is the largest one to be built so far and has the tightest requirements on angular resolution. A prototype mirror system of the Wolter type has been completed and the first mirrors for the flight telescope have been ground and polished. Another step forward in astronomical research will be made with the AXAF (Advanced X-ray Astrophysics Facility) which is currently planned in the United States of America. AXAF will utilise a Wolter telescope, the largest mirror having a diameter of 1.2 m. The angular resolution is specified at the sub-arcsecond level.

Since the discovery of the first non-solar x-ray source only 22 years have passed during which x-ray astronomy has grown to a mature astronomical research discipline. This fact is related to the ability to successfully build and launch imaging telescopes. As in optical or radio astronomy scientific progress in x-ray astronomy depends on the size and resolving power of the optics together with the development of efficient focal plane detectors with good spatial and/or spectral resolution. Since the fundamental work of Wolter no really new proposal has been made for a more advanced imaging system. As a consequence improvements have had to be made in the fields of mirror fabrication technology, surface metrology and in a better understanding of the physics of x-ray reflection and scattering. The purpose of this paper is to review the achievements which have been made so far. Although the term 'telescope' includes more than just the optics, the aspects of mechanical and thermal design of the structure, mounting schemes and stability problems will not be discussed in detail.

2. Reflection of x-rays from perfect mirrors

2.1. Theory of grazing incidence reflection

X-ray telescopes make use of the principle of grazing incidence reflection. The interaction of x-rays with matter can be described by the complex index of refraction of the reflector:

$$n = 1 - \delta - i\beta = \sqrt{\epsilon} \tag{2.1}$$

where δ describes the phase change and β accounts for the absorption. Instead of the index of refraction the complex dielectric constant ϵ may be used. The reflection coefficients for p and s polarisation are given by the Fresnel equations:

$$r_p = \left(\frac{E_R}{E_i}\right)_p = \frac{n^2 \sin\alpha - (n^2 - \cos^2\alpha)^{1/2}}{n^2 \sin\alpha + (n^2 - \cos^2\alpha)^{1/2}} \tag{2.2}$$

$$r_s = \left(\frac{E_R}{E_i}\right)_s = \frac{\sin\alpha - (n^2 - \cos^2\alpha)^{1/2}}{\sin\alpha + (n^2 - \cos^2\alpha)^{1/2}}. \tag{2.3}$$

E_R/E_i denotes the ratio of the amplitudes of the reflected and incident electric fields and α is the grazing angle of incidence as measured from the interface plane. This approach is, in principle, correct as long as the assumptions inherent in the Fresnel equations are fulfilled: the reflector is assumed to have a perfectly flat surface and its atomic structure scales are small compared to the x-ray wavelength used. The reflected intensity or reflectivity is then $R_p = r_p r_p^*$ and $R_s = r_s r_s^*$, where the asterisk denotes the conjugate complex value. In the case of incident unpolarised x-rays the reflectivity is $R = (R_p + R_s)/2$. Since the real part of n is less than unity for matter at x-ray wavelengths, total external reflection occurs at a grazing angle α_t according to Snell's law:

$$\cos \alpha_t = 1 - \delta \tag{2.4}$$

or for $\delta \ll 1$:

$$\alpha_t = \sqrt{2\delta}. \tag{2.5}$$

Because of the non-vanishing value of β the reflection is actually not total for $\alpha \leqslant \alpha_t$, but is less than unity, and x-rays are reflected at incident angles even larger than the critical angle α_t.

2.2. *Optical constants*

The index of refraction or the optical constants can be computed from anomalous dispersion theory. For x-ray wavelengths λ sufficiently apart from absorption edges δ reads as follows:

$$\delta = N_0 \frac{Z r_e}{A 2\pi} \rho \lambda^2 \tag{2.6}$$

where N_0 is Avogadro's number, r_e is the classical electron radius, Z and A are the atomic number and weight, respectively, and ρ is the mass density. In the case of heavy elements, for which Z/A is about 0.5, the critical angle for $\delta \ll 1$ can be estimated:

$$\alpha_t = 5.6 \lambda \sqrt{\rho} \tag{2.7}$$

with α_t in arcmin, λ in ångströms and ρ in g cm^{-3}. This means that for x-rays with a wavelength of a few ångströms the critical angle is about one degree. Equation (2.7) also shows the superiority of heavy elements like gold or platinum as x-ray reflectors. Therefore, efficient x-ray mirrors have to be coated. There are, however, exceptions from this rule if the heavy elements have absorption structures in the x-ray region of interest, like gold near 5.6 Å for example. There the reflectivity is greatly reduced and lighter elements such as nickel become more favourable. A better estimate of δ can also be obtained in the absorption edge region by using the full expression of the Kramers–Kallmann–Mark theory (Compton and Allison 1935).

Experimentally the index of refraction can be determined by measuring the reflectivity dependence on incidence angle and fitting the Fresnel formula to the data. This method has been used from the very early years (Forster 1928, Dershem and Schein 1931), and through the decades up to the present time (Hendrick 1957, Johnson and Wuerker 1963, Lukirskii *et al* 1964, Stewardson and Underwood 1965, Ershov *et al* 1967, Savinov *et al* 1970). Many different materials have been investigated at a variety of wavelengths. However, for particular elements like gold, data are rather scarce in the literature and, furthermore, for the samples measured, a large spread in reflectivity

has been reported, yielding unsatisfactory information about δ and β (Costa *et al* 1978, Aschenbach and Bräuninger 1978). Various effects arising from chemical contamination via oxidation or hydrocarbonate films, mass densities lower than the average bulk density of the reflecting surface, voids in the surface material and dust scattered across the surface have been considered to be the source of these discrepancies. Another possibility is microroughness scattering which will be discussed in § 3.3. A quantitative explanation is still lacking.

Kiessig (1931) used another experimental approach to determine the optical constants of nickel. He observed x-ray interference patterns when he illuminated a glass flat which was coated with a thin nickel layer. By changing the incidence angle the interference pattern changed, and from a calculation of the corresponding phase shifts the nickel layer thickness as well as δ can be determined. This method has since been used in thin-film technology to measure the thickness of thin layers. A very similar technique was used by Predehl *et al* (1981) and Tatchyn *et al* (1982). They have derived the optical constants for gold from measurements of the diffraction pattern of transmission gratings either by rotating a single grating or by comparing the individual diffraction patterns of two or more gratings. However, the results differ in a systematic way from results obtained by other methods and further work is required.

At rather long wavelengths ($\geqslant 80$ Å) electron energy-loss spectroscopy has been used to derive the dielectric constant (Daniels *et al* 1970, Schlüter 1972, Feldkamp *et al* 1979). This method uses the fact that the energy-loss spectrum of electrons passing through a thin film depends on its dielectric constant $\epsilon = \epsilon_1 + i\epsilon_2$ as $\epsilon_2/|\epsilon|^2$. ϵ_1 is determined via a Kramers–Kronig analysis.

Measurements of the absorption coefficient are used to derive both δ and β, applying the quantum dispersion relations (Henke 1981a). In this context the interaction of x-rays with matter is described by the complex atomic scattering factor $f_1 + if_2$. f_2 is related to the atomic absorption coefficient through the following:

$$f_2 = \frac{E\mu_a(E)}{2\pi r_e hc} \tag{2.8}$$

where E is the x-ray photon energy, μ_a is the atomic photon absorption cross section and r_e is the classical electron radius. The remaining variables are in accord with the standard notation of fundamental constants. f_1 can be expressed as follows:

$$f_1 = Z + \frac{1}{\pi r_e hc}\int_0^\infty \frac{x^2\mu_a(x)}{E^2 - x^2}\,dx + \Delta f_r \tag{2.9}$$

where Δf_r is a relativistic correction term which is negligible in the soft x-ray range. The following relations connect the atomic scattering factor with the optical constants:

$$\delta = \frac{N_0 \rho r_e}{A 2\pi}\lambda^2 f_1 \tag{2.10}$$

$$\beta = \frac{N_0 \rho r_e}{A 2\pi}\lambda^2 f_2 = \mu_a \lambda. \tag{2.11}$$

Thus, by measuring μ_a and exercising the above integral, also known as the Kramers–Kronig transform, δ and β can be determined. In this way Hagemann *et al* (1974) derived the index of refraction for a number of selected materials from the far-infrared to the x-ray region. The most extensive work in this area has been done by Henke and his collaborators. A recent compilation of the best available experimental and

theoretical μ_a data has been published by Henke *et al* (1982) for the energy region from 30 eV to 10 keV. They used these data to derive the atomic scattering factors for 94 elements covering the x-ray energy band from 100 eV to 2 keV (Henke 1981b). An extension of this method into the energy region of up to 10 keV has been accomplished by Zombeck (1983a) for the elements nickel, gold and platinum accompanied by reflection measurements.

This approach, using measured μ_a data and computed δ values, was adopted in a somewhat different manner by the early grazing incidence telescope designers. They used the Kramers–Kallmann–Mark anomalous dispersion theory to compute δ which resulted in sufficiently accurate predictions for the reflectivity (Giacconi *et al* 1969). With these reflectivity data at hand a reasonable estimate of the efficiency, i.e. the reflectivity, of any mirror system is possible, apart from the effects which are due to surface imperfections.

3. Reflection of x-rays from real surfaces

In the preceding section reflection from perfectly smooth mirror surfaces has been discussed. Real mirrors, however, show surface irregularities, which might be of a chemical or physical origin. The problem of mirrors chemically contaminated by either oxidation or adsorption will not be treated in this review. Physical imperfections related to the spatial structure of the surface give rise to an angular broadening of the image intensity distribution, with stray light appearing about the specular direction, i.e. the direction the beam should follow according to Snell's law.

Experimental studies on x-ray scattering properties of mirrors have been carried out by a number of investigators (Ehrenberg 1949b, Buteux 1953, Elliott 1963, Schroeder and Klimasewski 1968, Croce *et al* 1972, Lindsey 1973, Lindsey and Penfold 1976, Croce and Névot 1976). However, all these measurements were performed at short x-ray wavelengths between 1.5–1.9 Å and necessarily at small grazing angles. For x-ray telescopes longer wavelengths are more appropriate and scattering measurements have been reported by a few groups (Wriston and Froechtenigt 1973, Van Speybroeck 1973, Lenzen 1975, 1978, de Korte and Lainé 1979, Aschenbach *et al* 1980, 1981, Hasinger 1980, Zombeck *et al* 1981, 1982, Herring 1982, Williams and Reily 1984, Williams *et al* 1984). The primary purpose of these investigations on flat samples was and still is to select the mirror substrate materials and polishing methods most suitable to develop low-scatter high-resolution telescopes. Therefore these papers contain long lists of various substrates, including beryllium, aluminium, nickel, quartz glass, fused silica, float glass, ultra-low-expansion (ULE) glasses and glass ceramics like Zerodur, which have been prepared and polished with different techniques by different optical (mostly commercial) workshops. Apart from this pragmatic and preparatory work some of the data were compared with theory, which had been introduced by Lenzen (1978) for the first time. The theory used was wave scattering from statistically rough surfaces.

3.1. Scattering theories

The description of wave scattering by diffractive processes has been of great interest in electromagnetic and acoustic applications for a long time. In fact, the first mathematical investigation of the scattering of sound waves from rough surfaces dates back as far as 1878 when Rayleigh discussed the scattering of a plane wave by a sinusoid. A

variety of application problems have been solved in the context of radar scattering from topographic irregularities including the reflection from objects as distant as the planets. The theory is well developed so that extensive literature is available even in the form of text books (see, for example, Beckmann and Spizzichino 1963, Ishimaru 1978, Bass and Fuks 1979). In recent years this theory has been applied to shorter electromagnetic waves including the visible (for reviews see Welford (1977) and Elson and Bennett (1979)) and even to the x-ray range.

In general, two different approaches are used to formulate scattering theories, which are known as 'vector perturbation technique' and 'Kirchhoff approximation'. The latter theory is based on Kirchhoff's diffraction theory and specific problems are addressed by solving the Helmholtz integral. This approach is valid only as long as the radius of curvature of the irregularities is large compared to the wavelength. This results from the fact that Kirchhoff's boundary conditions are fulfilled if the shape of the rough surface can be approximated accurately enough by tangential planes whose extent projected on the incident wavefront is large compared to the wavelength. The second approach makes use of perturbation methods with the following expression for the perturbation term:

$$\Delta^2 = (2k\sigma \sin \alpha)^2 \tag{3.1}$$

where $k = 2\pi/\lambda$ is the wavenumber of the radiation and α is the grazing incidence angle. Δ is the phase difference between two rays which are specularly reflected from two adjacent areas on the surface. The vertical separation of the two areas is σ. Accordingly, a surface is called smooth if $\Delta^2 \ll 1$, which in fact is the Rayleigh criterion. For this size of imperfection the series expansion of the vector theory solutions can be terminated after the first term.

With either of these two theories it is possible to describe the scattering properties of statistically or random rough surfaces. The variation in height of a rough surface may be given by $z = f(x, y)$, where the xy plane is the mean surface level. The scattering geometry including the angular notations is given in figure 1. The following equations give the solution in the Kirchhoff approximation for a scalar wave field (Beckmann

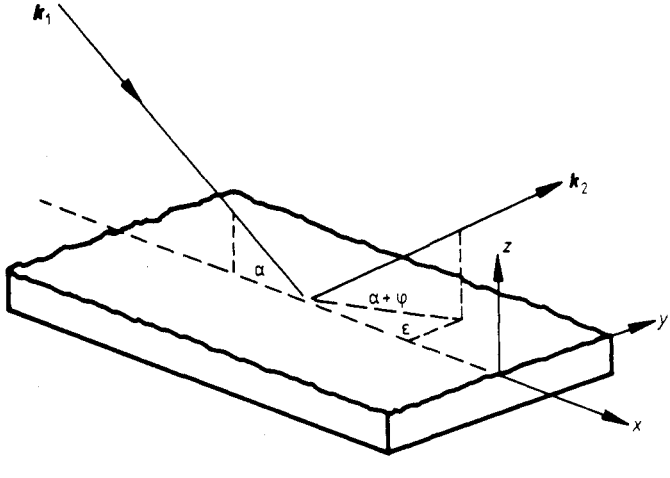

Figure 1. Scattering geometry. k_1 and k_2 denote the wavevector of the incident and scattered ray, respectively.

and Spizzichino 1963):

$$\frac{1}{I_0}\frac{\mathrm{d}I}{\mathrm{d}\omega}=\frac{2\pi F^2}{A}\sum_{m=1}^{\infty}\frac{g^m}{m!}\int_0^{\infty}J_0(v_{xy}\tau)C^m(\tau)\tau\,\mathrm{d}\tau \tag{3.2}$$

$$F=\frac{1+\sin\alpha\sin(\alpha+\varphi)-\cos\alpha\cos(\alpha+\varphi)\cos\epsilon}{\sin\alpha[\sin\alpha+\sin(\alpha+\varphi)]} \tag{3.3}$$

$$g=\{k\sigma[\sin\alpha+\sin(\alpha+\varphi)]\}^2 \tag{3.4}$$

$$p=k[\cos(\alpha+\varphi)\cos\epsilon-\cos\alpha] \tag{3.5}$$

$$q=k\cos(\alpha+\varphi)\sin\epsilon \tag{3.6}$$

$$v_{xy}^2=p^2+q^2. \tag{3.7}$$

In addition to the quantities already defined, the further notation used is I_0, totally reflected (specular reflected and scattered) flux; ω, scattering solid angle; σ, RMS surface roughness as derived from $f(x, y)$; J_0, Bessel function of zero order; $C(\tau)$, autocorrelation function of $f(x, y)$; and A, normalisation factor.

The gradient of $f(x, y)$ at each surface locus is assumed to be small compared to the mean grazing angle, so that the microscopically varying reflectivity can be represented by the Fresnel reflectivity for the mean grazing angle. The validity of the result given above is unrestricted in roughness level. The result has, however, been derived for a Gaussian distribution of the surface heights and an isotropic rough surface. In this case the total integrated scatter is

$$\frac{I_s}{I_0}=\frac{1}{I_0}\int\frac{\mathrm{d}I}{\mathrm{d}\omega}\,\mathrm{d}\omega=1-\exp[-(2k\sigma\sin\alpha)^2]=1-\exp(-\Delta^2). \tag{3.8}$$

From first-order vector theory the intensity distribution of the scattered light is given by the following expression (Church *et al* 1979):

$$\frac{1}{I_i}\frac{\mathrm{d}I}{\mathrm{d}\omega}=4k^4\sin\alpha\sin^2(\alpha+\varphi)QW(p,q) \tag{3.9}$$

where I_i is the incident intensity. Q depends on the index of refraction and the polarisation of the incident beam and it reduces to the Fresnel reflection coefficient for small scattering angles. $W(p, q)$ is the power spectral density of $f(x, y)$. This solution is valid in the smooth surface limit but it is not restricted to isotropic surfaces. The total integrated scatter amounts to Δ^2, which is also obtained from the scalar theory in the Kirchhoff approximation for $\Delta \ll 1$. This result allows one to derive the surface roughness σ from total integrated scattering (TIS) measurements. Bennett and Porteus used this relation as early as 1961 to quantify the roughness of optical surfaces.

It is interesting to compare the results of the two theories. In order to do so, one has to assume $\Delta \ll 1$. In this case the series in equation (3.2) can be terminated after the first term. The residual integral over the correlation function is the Hankel transform of the isotropic power spectral density (Church *et al* 1979). Therefore both theories show the same dependence on the surface properties. If the normalisation factor A is chosen as λ^2/α both theories predict exactly the same results for $\alpha, \varphi \ll 1$ (Hasinger 1980), although the solution in equation (3.2) was derived for a scalar field. For larger scattering angles vector perturbation theory shows a pronounced difference in the scattering distribution with polarisation (Rehn *et al* 1980).

The scattering distribution can be completely described by statistical functions like the power spectral density of the surface deviations. The power spectral density is defined as

$$W(p, q) = \frac{1}{S}\left|\int \mathrm{d}x \int \mathrm{d}y \exp\left[\mathrm{i}(px + qy)\right] f(x, y)\right|^2 \tag{3.10}$$

where S is the illuminated surface. This means that the surface deviations are Fourier-decomposed and the power spectral density measures the distribution of spatial surface wavelengths $\mathrm{d}x$ and $\mathrm{d}y$ with $p = 2\pi/\mathrm{d}x$ and $q = 2\pi/\mathrm{d}y$. In this sense the scattering distribution traces the surface microtopography and vice versa. In principle, the scattering distribution can be predicted if the power spectral density can be derived from mechanical stylus measurements or other means sensitive in the region of the spatial wavelengths of interest. The correlation between scattering and surface spatial wavelength is even more close. The incident wave is diffracted by each particular Fourier component of spatial wavelength d according to the grating equation:

$$\cos(\alpha + \epsilon_m) - \cos\alpha = m\lambda/d. \tag{3.11}$$

Whereas the zeroth order corresponds to the specular direction the higher orders contain the scattered light. For smooth surfaces with $\Delta \ll 1$, significant intensity is only in the first orders and equation (3.11) reduces to

$$\epsilon = \frac{\lambda}{d \sin\alpha} \tag{3.12}$$

for small diffraction angles ϵ.

Accordingly, scattering angle and spatial wavelengths are related to each other for fixed α and λ. Some numerical examples may illustrate the relation for x-rays, i.e. a wavelength of 10 Å and a grazing angle of 1°. Scattering towards 1° is caused by $d \sim 3\ \mu$m, 1 arcmin scattering by $d \sim 200\ \mu$m and 1 arcsec by 1.2 cm. The second consequence of the grating equation is that any scattering measurement limited to an angular band is also band-limited in d. This is important to keep in mind in the interpretation of scattering data and topographic surface measurements when taken with different devices, as pointed out by Church and Zavada (1975) and Church (1979).

3.2. Experimental results

Very detailed measurements of the soft x-ray scattering properties of mirrors have been performed by Lenzen (1978). Soft x-ray scattering measurements have to be carried out in vacuum because of the high absorption of air. A diagram of a typical set-up is shown in figure 2. Characteristic line radiation is generated in an open x-ray tube with replaceable anodes. Thin-film absorption filters suppress most of the bremsstrahlung continuum. The flux of the direct beam and its time variation is monitored by a proportional counter. Collimation of the beam of typically 0.5 arcmin FWHM is made using either a slit or pinhole system. The mirror sample is mounted on a remotely controlled holder allowing adjustment of angles and position. The reflected beam is scanned by means of an exit slit in front of a low background proportional counter. Figure 3 shows a collection of scattering distributions which Lenzen (1978) obtained for a Kanigen surface on an aluminium substrate of comparatively high scattering level. This is a one-dimensional distribution integrated over the direction perpendicular

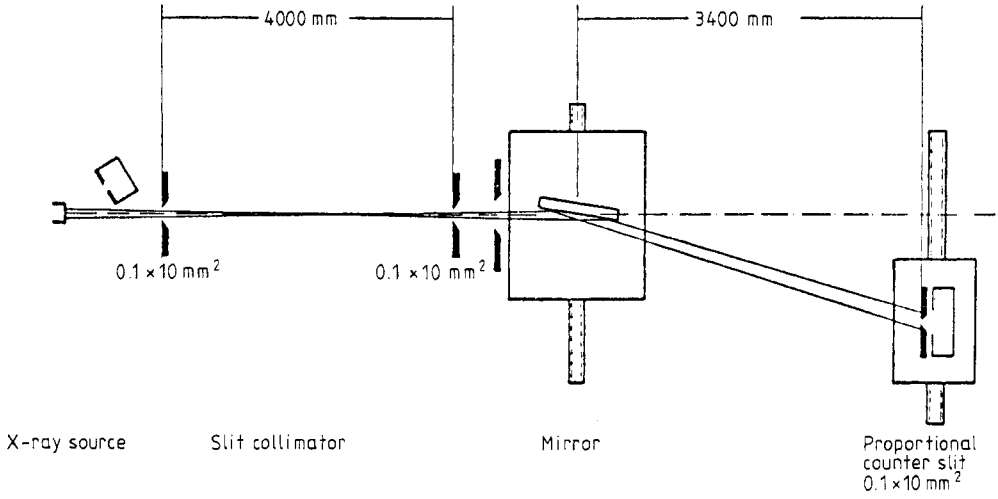

Figure 2. Typical experimental set-up to carry out angle-resolved scattering measurements.

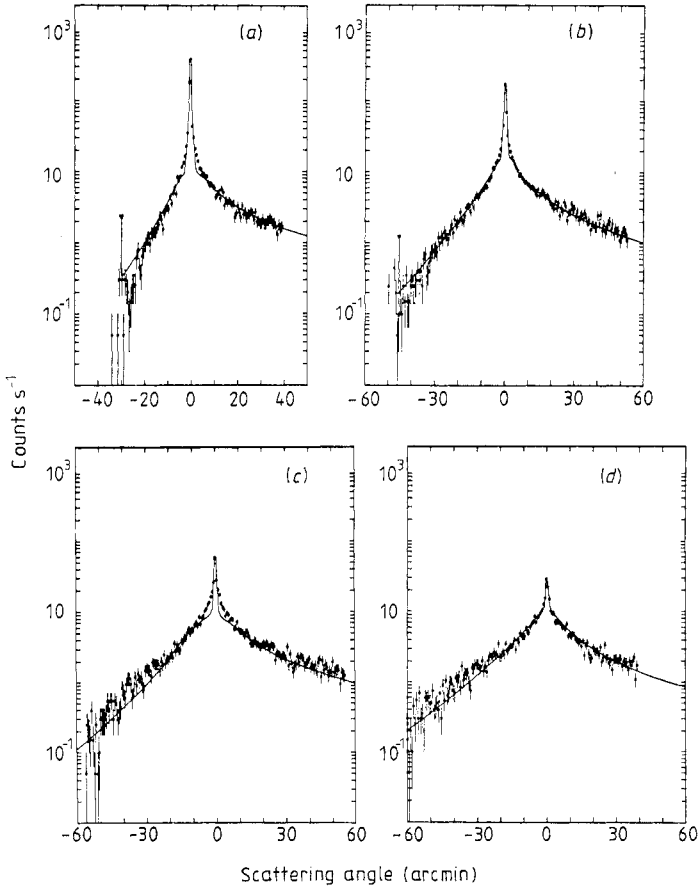

Figure 3. Comparison of measured and theoretical scattering distributions in the plane of incidence of a Kanigen flat sample at $\lambda = 13.3$ Å for grazing angles $\alpha = 0.5°$ (*a*), 0.75° (*b*), 1.0° (*c*) and 1.25° (*d*) (Lenzen 1978).

to the plane of incidence. Two components are visible in the diagrams: the centre is dominated by the shape of the direct beam, and scattering wings extend out to more than a degree. By integrating the distribution from 15 arcmin to 60 arcmin and extrapolating outside, Lenzen has derived the total integrated scatter (TIS). Figure 4 shows the TIS data plotted against grazing angle for different x-ray wavelengths as well as the theoretical expectations derived from equation (3.8) by fitting the microroughness parameter σ. From this and other samples, the exponential form for the TIS was found to be valid in the x-ray regime over a wavelength band from 8.3-44 Å, grazing angles from 0.5-3° and microroughness levels from 6-120 Å. Outside these bands no measurements were made.

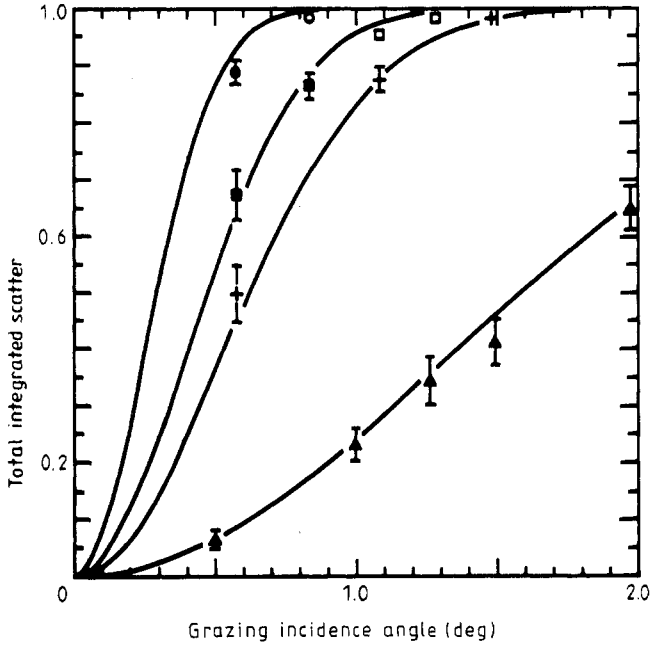

Figure 4. Total integrated scattering data plotted against grazing incidence angle at various x-ray wavelengths. The full curves are derived from scattering theory with a single common value for the microroughness (Lenzen 1978). Values of λ (Å): ○, 8.3; □, 13.3; +, 17.6; ▲, 44.8.

One sample has been prepared on purpose with a relatively large microroughness ($\sigma \sim 110$ Å) to enable the study of the shape of the scattering angular distribution using scalar theory as given in equations (3.2)-(3.7). An exponential autocorrelation function has been found to provide acceptable fits in the angular range beyond about 5 arcmin. The fitted curves are superimposed on the data as full curves in figure 3. In the very central part deviations from this behaviour are sometimes apparent. The correlation length for this particular sample turned out to be 10 μm. By using the grating equation, the minimum and maximum spatial wavelengths are derived as 3.5 μm and 350 μm, respectively. Deviations of the autocorrelation function from the exponential mentioned above occur for spatial wavelengths $\geqslant 100$ μm. It is interesting to note that Gaussian or Lorentzian autocorrelation functions do not fit the data acceptably.

Lenzen also investigated the scattering distribution perpendicular to the plane of incidence, which he found to be much narrower than in the plane of incidence. The

distribution in this direction was indistinguishable from the shape of the direct beam which is consistent with the scattering theories predicting a distribution narrower by a factor of sin α.

Similar measurements on highly polished Zerodur flats have been carried out by Hasinger (1980). Independent of the coating (no coating, nickel, gold, platinum) the samples exhibit an extremely low level of microroughness down to 2.3 Å. Again, a uniquely determined value for σ as well as for the autocorrelation length with an exponential distribution can be ascribed to each sample. Statistically acceptable agreement between scattering theory and measurement has been found for grazing angles between 15–150 arcmin, x-ray wavelengths between 1.9–13.3Å and scattering angles between 5–20 arcmin (cf figure 5). As in the measurements of Lenzen, the data show that the scattering distributions rise more rapidly towards the core than that of an exponential autocorrelation function with an average length of a few microns would imply.

Detailed x-ray scattering measurements on flat samples have also been carried out by de Korte and Lainé (1979). The experimental set-up is very similar to the one shown in figure 2. They report the scattering results of 14 different samples with no significant differences in polishability for Zerodur, Suprasil, glass and Kanigen. The quality criterion was the value for σ derived from the fractional scattered flux within

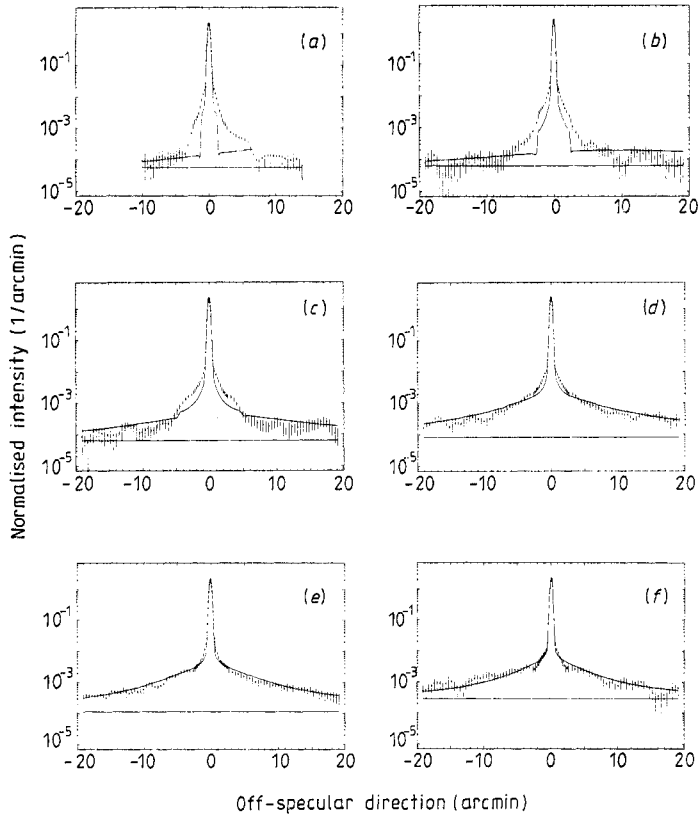

Figure 5. Comparison of measured and theoretical scattering distribution in the plane of incidence for a highly polished Zerodur flat sample at $\lambda = 8.3$ Å for grazing incidence angles 15 arcmin $\leq \alpha \leq$ 150 arcmin (Hasinger 1980). (*a*) 15 arcmin, (*b*) 30 arcmin, (*c*) 60 arcmin, (*d*) 90 arcmin, (*e*) 120 arcmin, (*f*) 150 arcmin.

the band from 45 arcsec to 12 arcmin off the specular direction, using first-order vector theory. σ varies between 2.7–12 Å among the different samples.

To explore the region within a few arcmin of the specular direction, x-ray measurements with high angular resolution have been carried out in the 130 m long beam test facility of the Max-Planck-Institut für Extraterrestrische Physik (MPI). The facility has been designed and built to test and calibrate the Rosat telescope. It has already been used for extensive calibration of the Exosat qualification and flight models. A description of the facility is given by Aschenbach *et al* (1979) and Stephan *et al* (1981). Figure 6 shows an aerial view of the facility. For the measurements of flat mirror samples, the facility has been set up as shown in figure 7. With a collimator split system (the slits being 100 m apart and each 100 μm wide), the residual divergence of the direct beam is 2.5 arcsec FWHM, which is primarily due to the size of the focal spot of the x-ray source. Scattering measurements have been made in two different modes. For low grazing angles of less than 23 arcmin the reflected beam remains within the vacuum pipe after a single reflection. For larger grazing angles where the beam would otherwise hit the walls of the pipe, a second reflection is utilised to bring the beam back into the system. This mirror periscope configuration is shown in the insert of figure 7.

In order to investigate the scattering close to the specular direction a sample has been tested which had not been polished to a superfinish but being simply of good optical quality. It is made of a quartz glass called Homosil. Figure 8 shows the scattering distribution displayed over ±75 arcsec for a wavelength of 8.3 Å. Single-reflection measurements at grazing angles of 23 arcmin as well as double-reflection measurements at 23, 39 and 51 arcmin are available. For comparison, the profile of

Figure 6. Aerial view of the x-ray test facility (PANTER) of the Max-Planck-Institut für Extraterrestrische Physik. The 130 m long, 1 m diameter vacuum pipe extends from the upper left to the lower right in the photograph.

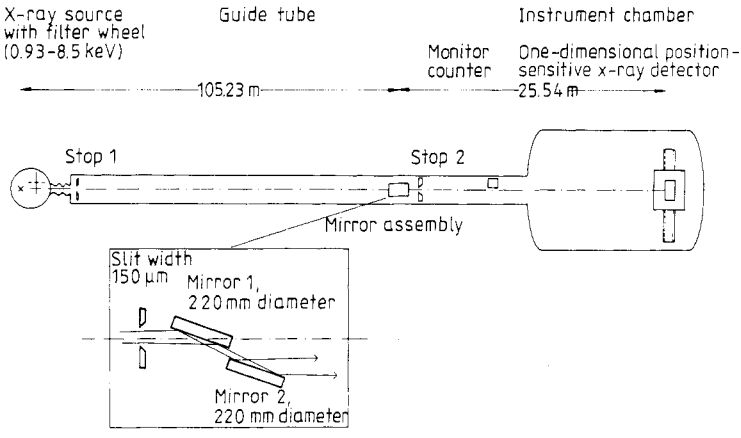

Figure 7. Schematic of the set-up used for high-resolution scattering measurements at the PANTER 130 m long beam test facility.

the direct, unreflected beam has been included in each graph normalised to the total counts recorded from the scattering measurement. Scattering is clearly present in the data over the entire angular range even in the arcsec region. At 23 arcmin grazing angle the scattering at single reflection is rather low and is significantly higher at double reflection as expected. Unfolding the profile of the direct beam the width of the scattering distribution is ~1 arcsec FWHM, independent of single or double reflection.

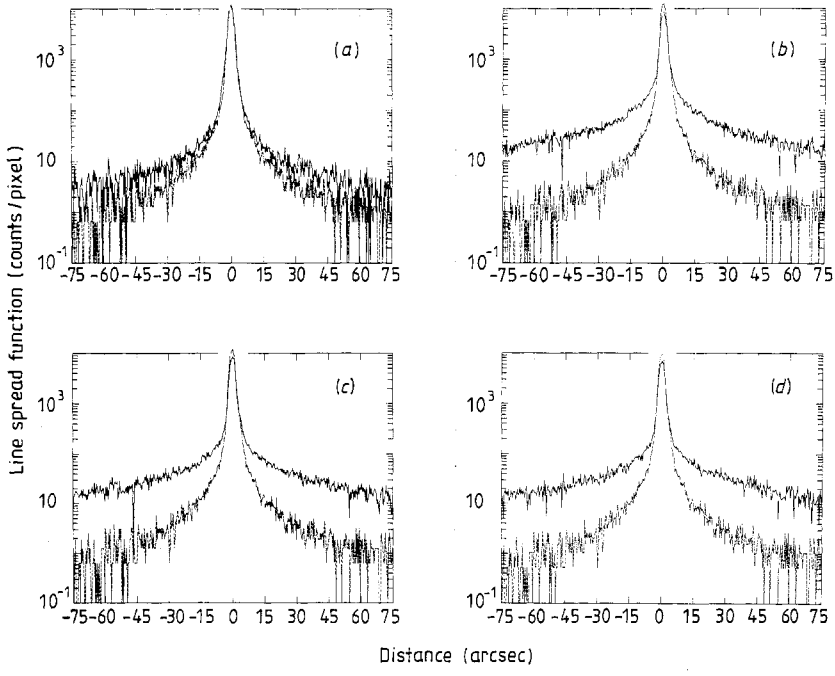

Figure 8. Scattering distributions of a Homosil flat sample measured in the plane of incidence at $\lambda = 8.3$ Å (full curve). The broken curve corresponds to the profile of the direct beam. (*a*) is taken at a grazing angle of $\alpha = 23$ arcmin and single reflection. (*b*), (*c*) and (*d*) result from double reflection at $\alpha = 23$, 39 and 51 arcmin, respectively.

The angular width containing 50% of the reflected intensity is ~1 arcsec for single reflection and ~1.8 arcsec for double reflection. Surprisingly, the scattering distributions show very little change, if any, with varying grazing angle. This has already been noticed in the scattering distributions taken at lower resolution as a wavelength-independent excess. The origin of this excess is unexplained.

Within the AXAF technology programme 35 highly polished optical flats have been subjected to extensive x-ray scattering tests. The mirror substrate materials included ULE, Cervit, Zerodur and nickel beryllium. The surfaces were coated either with Ni, Au or Pt. The samples were tested at the 300 m long beam x-ray test facility of the Marshall Space Flight Center. Originally, the facility had been constructed to calibrate the Einstein telescope. The measurement set-up is very similar to the MPI long beam set-up, except it is longer and the mirror periscope fixture can be placed at a distance of ~180 m from the image detector, thereby providing higher angular resolution. In these tests the resolution was limited by the detector pixel element to 0.17 arcsec. Measurements were performed at wavelengths of 4.15, 1.9 and 1.53 Å for angles of incidence of 25, 39 and 51 arcmin. The majority of the flats showed extremely low scatter. Typically 50% of the reflected energy was within a circle of $\leqslant 1.2$ arcsec diameter, and the 90% encircled energy diameter was ~5 arcsec (Williams *et al* 1984, Williams and Reily 1984). However, the authors concluded from the low value for the integrated reflectivity that some fraction of the scattered flux was outside the field of view of 5 arcmin of the image detector. This would be explained by surface irregularities with spatial wavelengths between 5-10 μm. Measurements over an extended range of scattering angles are necessary for clarification.

A subset of the samples was also tested at the MPI long beam test facility (Zombeck *et al* 1981, Zombeck 1982). Although tested at somewhat lower resolution and at longer wavelengths up to 8.3 Å the conclusions are as above. A detailed comparison with scattering theory was hampered by the extremely low scattering level. Flats with graded roughness are necessary to test the theory. In both investigations several flats have been found which showed poor figure far from flatness, although they had been highly polished. It remains to be seen to what level both the requirements of good figure and excellent finish can be met simultaneously.

Whereas the measurements presented so far have been made exclusively in the context of astronomical application programmes there is now growing interest in x-ray mirrors with the introduction of large synchrotron facilities. Results of angle-resolved scattering measurements obtained at a beam line of the Stanford Synchrotron Radiation Laboratory have been reported by Rehn *et al* (1980) and Elson *et al* (1980). Due to the synchrotron origin of the x-rays the measurements could be made with polarised light. Unfortunately, the mirror samples tested showed large surface roughness so that comparison with first-order vector theory was precluded.

3.3. Impact of surface scattering upon reflectivity

It was pointed out in § 2.2 that there is a large spread in reflectivity data obtained from flat x-ray mirror measurements by different experimenters. One possibility which has been discussed recently could lie in the surface roughness differing from sample to sample. Aschenbach and Bräuninger (1978) have presented results of grazing incidence reflectivity measurements for gold-coated flat samples in the wavelength range from 8.3-44 Å. Three different substrate materials have been studied including Zerodur, Kanigen and Nibodur, the latter being a glass. The reflectivity of the samples

differ significantly in a systematic way for all wavelengths and grazing angles investigated. The results at 44 Å have been reproduced in figure 9. The ratio of the Zerodur to the Kanigen reflectivity follows an exp $(-\alpha^2)$ dependence for grazing angles $1.5° \leqslant \alpha \leqslant 8°$. According to the results of § 3 this is indicative for surface scattering and the result could be explained if the Kanigen surface had a RMS roughness of ~30 Å with an autocorrelation length of ~1 μm. Unfortunately, there is no independent measurement of the surface roughness available.

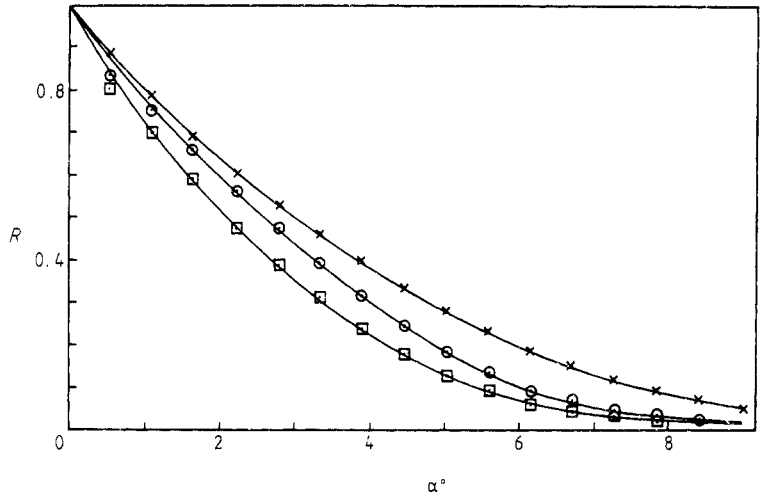

Figure 9. Measurements of the reflectivity plotted against grazing angle taken at $\lambda = 44.8$ Å for three different polished flat samples: Zerodur (×), Kanigen (⊙) and Nibodur (⊡). Full curves result from a best fit using the Fresnel formulae with the optical constants as given below:

	δ ($\times 10^4$)	β ($\times 10^4$)
×	60.66 ± 0.44	76.65 ± 2.76
⊙	40.27 ± 1.07	37.73 ± 3.40
⊡	30.17 ± 0.50	41.17 ± 3.13

Further evidence for a dependence of reflectivity upon surface roughness comes from scattering measurements of the MPI grazing incidence telescopes. Three identical Wolter telescopes of 32 cm aperture have been available for investigation and x-ray pencil beam tests have been performed on a series of different areas of individual telescopes. The reflectivity plotted against scattering level for four distinct wavelengths is shown in figure 10. Clearly, there is a tendency for reflectivity to increase with decreasing scattering, which is accentuated by the broken line. Furthermore, extrapolating the correlation line to zero scattering the theoretically expected reflectivity is matched. Standard scattering theories as outlined before cannot explain this behaviour.

A very appealing attempt to include reflectivity losses for rough surfaces into a theory has been put forward by Névot and Croce (1975, 1980). They describe the reflection interface not as infinitely sharp with an unique and constant index of refraction but as a transition zone of finite depth within which the index of refraction gradually changes from unity at the top to the value of the solid reflector at the bottom. The change of the optical constants is related to the mass density averaged in planes

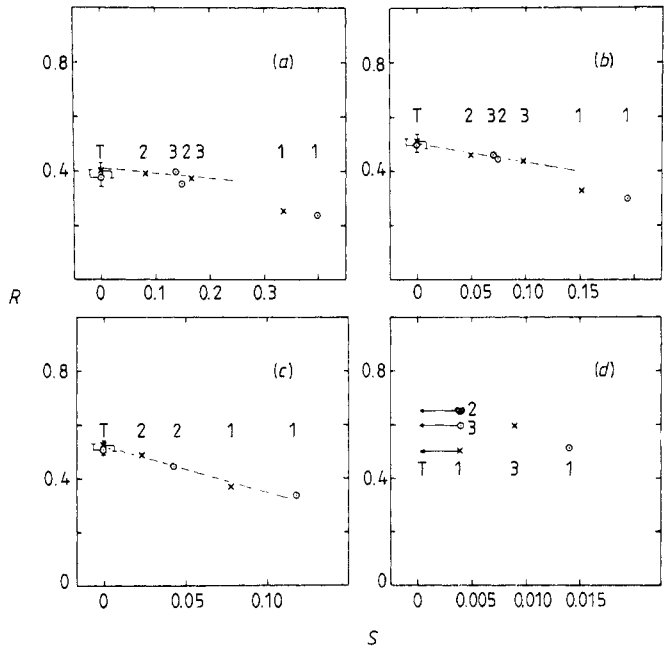

Figure 10. Measurements of reflectivity R plotted against total integrated scatter S for the three MPI Wolter-type telescopes, denoted by 1, 2 and 3, at four different wavelengths: (*a*) 8.34 Å, (*b*) 13.3 Å, (*c*) 17.6 Å, (*d*) 44.8 Å. Two measurements were performed on each telescope, differing in surface location (×, ⊙). T denotes the theoretically expected reflectivity for zero scattering, with error bars indicating an assumed ±10% uncertainty in the optical constants.

parallel to the mean surface and is therefore directly correlated with the microroughness. But because of the averaging the angular distribution of the scattered light cannot be derived. By means of this gradient index approach Bilderback (1981) successfully fitted measured x-ray reflectivity curves of a platinum-coated float glass over the x-ray energy range from 3.8–50 keV.

A very similar approach to the description of the reflection from a rough surface has been made by Smirnov *et al* (1979). In a subsequent paper by Smirnov (1980) the theory was expanded to also allow for scattering, by including density variations across the surface plane. Experimental data obtained from angle-resolved scattering measurements for a roughened glass plate at $\lambda = 1.94$ Å could be fitted by the model assuming a RMS roughness of ~160 Å. Independent measurements of the microtopography would be essential for testing this theory. In conclusion, it is likely that an increased scattering level reduces reflectivity and thus the straightforward derivation of the optical constants via the Fesnel formulae is appropriate only if mirror samples of very high surface finish are used.

4. Grazing incidence telescopes

In the previous sections the physics of reflection from a perfect mirror surface as well as the additional complications arising from surface scattering have been presented. The following sections deal with the design and realisation of grazing incidence

telescopes. But before doing so, it should be noted that other telescopes based on different physical principles have been constructed. These include pinhole cameras, Fresnel zone plates and multi-layer-coated mirrors. The zone plate can be thought of as a circular diffraction grating which consists of concentric alternately opaque and transparent zones with a radially monotonic decreasing width. Zone plates have successfully been used in solar research, and first images of the Sun have been reported by Bol Raap *et al* (1969) and Bräuninger *et al* (1971). The use of zone plates for observations of non-solar objects is certainly rather limited because of the combination of their small apertures and the low photon flux of cosmic x-ray sources. However, microscopy is expected to benefit from them. Schmahl *et al* (1981) reported the fabrication of zone plates by which a resolution of 500 Å has been achieved at an operating wavelength of 45 Å.

The traditional way of imaging is, of course, to use mirrors at normal incidence. However, because the index of refraction is so very close to unity the intensity reflectivity is 10^{-4} for $\lambda \leqslant 50$ Å, even for the most efficient reflectors. Nonetheless, the amplitude reflectivity is $\sim 10^{-2}$ and a high peak reflectivity could be achieved by a multi-layer stack which provides constructive interference at each interface. This occurs if the Bragg equation is fulfilled for each layer pair of thickness d in a periodic configuration:

$$2d \sin \alpha = m\lambda \tag{4.1}$$

where m is the diffraction order and α is the grazing incidence angle. For ~ 100 layer pairs the reflectivity would approach unity in the sample picked. Absorption, however, limits the peak reflectivity to 40–50%, as calculated from standard optical multi-layer theory. The Bragg equation shows that near normal incidence the layer thickness has to be comparable with the x-ray wavelength, thus requiring a coating technique feasible to produce ~ 10 Å thick layers. These techniques have been developed primarily by Spiller (1981) and Barbee (1981). Typical multi-layers are made up of a highly reflecting material like tungsten or nickel and a low absorption spacer material like carbon. Quite a number of coated flats have been produced and measured with satisfactory results. In fact, successful soft x-ray imaging has been performed in the laboratory with spherical multi-layer mirrors at normal incidence, enabled by either mechanical bending of a multi-layer-coated flat into spherical shape (Underwood and Barbee 1981) or by direct coating of a spherical mirror (Henry *et al* 1981). In addition to the high peak reflectivity these multi-layer designs feature a narrow wavelength passband $\Delta\lambda$ only within which the reflectivity is essentially non-zero. This is due to the constructive interference requirement which is invalidated for $\Delta\lambda \geqslant \lambda/10$. Multi-layer coatings can, of course, also be used on grazing incidence mirrors to extend the spectral coverage far beyond the critical grazing angle limitations. Catura *et al* (1983) have calculated the reflectivity of a multi-layer-coated grazing incidence telescope whose prime photon energy range is about 1 keV, based upon the grazing angles chosen in the design. A gold-carbon multi-layer increases the reflectivity between 6–7 keV from essentially zero to appreciable values. Even at photon energies as high as 25 keV a decent reflectivity can be obtained. Similar calculations have been carried out by Voglmaier (1984) for the Rosat telescope which demonstrated that an effective collecting area of ~ 100 cm^2 between 6–7 keV can be obtained. Zombeck (1983a) computed for the AXAF grazing incidence mirrors that even a two-layer coating consisting of a thin (100 Å) nickel film on top of a thicker gold surface can enhance the reflectivity significantly between 6–7 keV. Despite the technical problems still to be solved, such as diffusive interaction between the interfaces, multi-layer mirrors seem to have great

potential for future telescopes. The most powerful telescopes built so far, however, have made use of grazing incidence reflection from single layers and they will be described in the following.

4.1. Telescope configurations

There are three different configurations of objectives available working at grazing incidence which are called (i) the Wolter-type systems, (ii) the Kirkpatrick–Baez-type systems and (iii) the focusing collimator or 'lobster-eye' systems. Whereas the first two designs have been realised many times by now and also used for astronomical observations, the last has never been put into practice. From this point in the review the common practice of substituting 'telescope' for 'objective' will be followed.

4.1.1. Wolter telescopes. In 1952 Wolter published a paper (1952a) in which he discussed x-ray imaging grazing incidence mirror systems. The basis of his considerations was that the quality of an imaging device would be better the closer the Abbe sine rule is fulfilled. For rays parallel to the system optical axis this can be put as follows. The crossing point of the extension of each incident ray with the backwards extension of the corresponding focused ray has to lie on a sphere centred on the image focus. This sphere is called the principal surface. For a single mirror the principal surface is identical with the mirror surface itself. Since grazing incidence is required for efficient reflection a single mirror can never produce an image, whatever shape it has. There are, of course, single mirrors which can focus x-rays like the remote off-axis zones of a paraboloid. Off-axis rays, however, which are inclined to the rotational axis of the paraboloid are reflected into an annulus centred on the focus of the paraboloid. This large aberration is coma and, as Wolter has shown, can be overcome only by utilising a second reflection on a second mirror. Figure 11 is a schematic of the three configurations Wolter studied in detail and which are known as the Wolter type I, type II and type III systems. For each of the three configurations the two mirrors are arranged coaxially and they have a coincident common focus which makes the system focus. The Wolter type I and Wolter type II configurations both utilise a paraboloid and a hyperboloid. Within the type I system reflection occurs on the internal surfaces of each mirror; the reflection is off the external surface of the hyperboloid for the type II systems. In fact, the type II system is the grazing incidence analogue of the Cassegrain telescope. In type III systems the incident rays are first reflected from the external surface of a paraboloid and then focused by the internal surface of an ellipsoid.

The main difference between the three systems is the ratio of focal length to total system length. The focal length of the type I system is given by the distance from the paraboloid/hyperboloid intersection plane to the focus. Therefore the system length is larger than the focal length by the length of the paraboloid. The type II has a focal length which is larger and can exceed the system length substantially. The type III system has the shortest focal length of all three configurations. All three systems are equivalent in optical performance with respect to the Abbe sine condition. The principal surface is not a sphere as required but a paraboloid which is well approximated by a sphere in the angular region close to the centre of the field of view. Wolter showed that the sine condition can be approximately fulfilled also for larger apertures by introducing further hyperboloids, but only for an even number of mirrors in total.

In a second paper Wolter (1952b) took his analysis one step further and presented telescopes which exactly obey the sine condition, so that these systems are completely

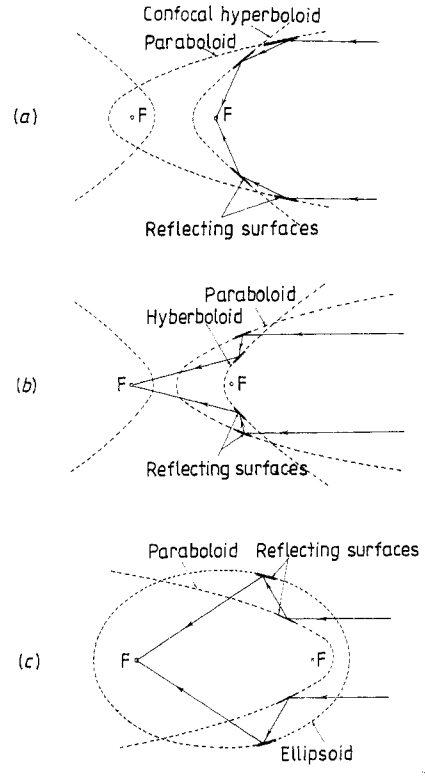

Figure 11. Schematic of the different Wolter telescopes called type I, type II and type III from top to bottom (Giacconi *et al* 1969).

free of spherical aberration and coma. This is achieved by a very small deviation of the mirror surfaces from their nominal second-order shape. The exact surface figure has been derived by Wolter by extending the solutions to grazing incidence which Schwarzschild already obtained for normal incidence in 1905. Therefore, these systems carry the name Wolter-Schwarzschild telescopes. Like the ordinary Wolter type systems three types are possible, differing in focal length to system length and in the utilisation of internal and external surfaces.

Whereas the image of an infinitely distant point source on the optical axis would again form a point in the image plane of a perfect Wolter or Wolter-Schwarzschild telescope—apart from aperture diffraction effects—a point-like object inclined to the optical axis by a field angle is imaged into a blur circle whose angular size is small compared to the field angle. Geometric aberration theory describes the dependence of the blur circle size on the various system parameters as a function of field angle. For mirrors which form a full figure of revolution standard optical aberration theory can be used even for grazing incidence (Cash *et al* 1979). Therefore, the aberrations can as usual be expanded into a power series. Accordingly, the first-order Gauss terms, the third-order Seidel terms and higher terms can be distinguished, including spherical aberration, coma, astigmatism, distortion and field curvature. The dominant aberration is field curvature. An analytic approach has been followed by Wolter himself (1971) and Winkler and Korsch (1977). In the majority of cases however, the aberrations have not been calculated analytically but by means of ray tracing, in which the path

of an ensemble of individual rays is followed geometrically throughout the mirror system. A systematic ray tracing study has been done by Van Speybroeck and Chase (1972) for Wolter type I systems and by Chase and Van Speybroeck (1973) for Wolter-Schwarzschild type I systems, deriving empirical relations for the blur. A ray tracing study aimed at a particular design, namely the S-056 ATM Skylab telescope, has been presented by Mangus and Underwood (1969). Ray tracing calculations have also been performed by Mangus (1970) to optimise a particular design for a Wolter type II system. The ray tracing technique has meanwhile become the standard method for the design and optimisation of any kind of telescope. It is particularly useful to include the treatment of perturbed surfaces. Werner (1977) has compared the performance of Wolter and Wolter-Schwarzschild type I systems with mirrors whose shape is described by high-order polynomials. By using appropriate polynomials the weight of the individual contributions to the total aberration can be changed and can lead, for example, to an almost flat field response, however, at the expense of on-axis performance. As pointed out by Cash *et al* (1979) by considering a few samples, the gain in off-axis resolution is not significantly greater than by simply shifting the flat Gaussian image plane towards the rear of the mirror system. Finally, Korsch (1979) has investigated the degradation in imaging performance which results if the primary paraboloid is replaced by a straight conicoid, which may ease fabrication.

The geometric photon collecting area of a grazing incidence telescope is the projection of the primary surface onto the aperture plane, thus forming a thin annulus. The collecting area can be enlarged by nesting additional Wolter telescopes in the interior, a technique already suggested in the early paper by Giacconi and Rossi (1960).

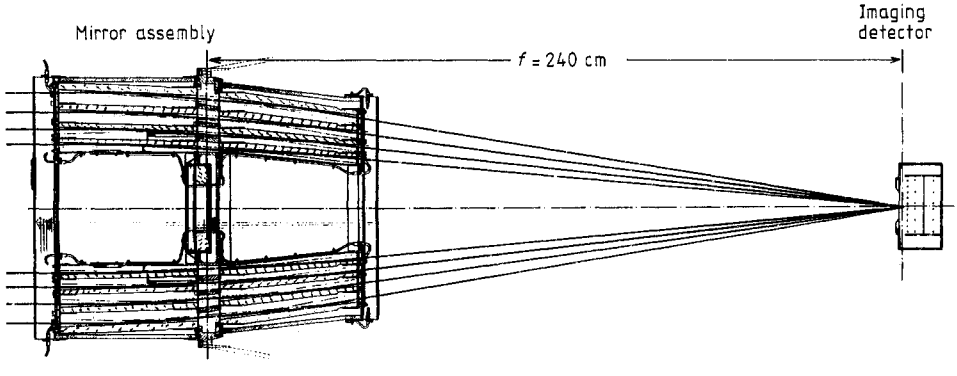

Figure 12. Schematic cross section of the Rosat telescope showing the four nested Wolter type I mirror systems.

Figure 12 shows a schematic of the Rosat mirror assembly which consists of a nest of four Wolter type I telescopes. Each system acts independently from its neighbouring ones. All four systems are coaxial and have a common system focus. Mainly because of engineering reasons the axial length of the individual components has been chosen in such a way that the front ends of the primaries form a common entrance plane and that the rear ends of the secondaries form a common exit plane. The radial size possible for an individual shell is determined by the geometry of the adjacent outer shell such that the exit ray bundle of this shell is not obstructed. In addition, each of the four mirror systems is designed such that a minimum spread amongst all principal surfaces is obtained, fulfilling the Abbe sine rule as closely as possible.

4.1.2. Kirkpatrick-Baez telescope. The first two-dimensional x-ray image ever obtained in the laboratory with grazing incidence reflection was taken by a Kirkpatrick-Baez system (Kirkpatrick and Baez 1948a, b). The configuration is shown in figure 13. The incident rays are focused to a line image by a parabolic sheet mirror. If the rays are reflected a second time from a parabolic surface oriented at right angle to the first one, a point-like focus is achieved. This is true for rays parallel to the centre line of the parabolas. In order to increase the collecting area a stack of parabolas of translation is constructed (see figure 13(*b*)). Whereas in the case of only one double plate system a perfect focus for on-axis rays can be achieved this is not possible for a multiple plate arrangement, where the focus remains perfect only along the projected direction of the surface normal of the primary. The exact solution for the intersection point with the focal plane of an arbitrary incident ray is given in the paper by Van Speybroeck *et al* (1971). A detailed configurational analysis of the multi-plate Kirkpatrick-Baez system has been carried out by Kast (1975).

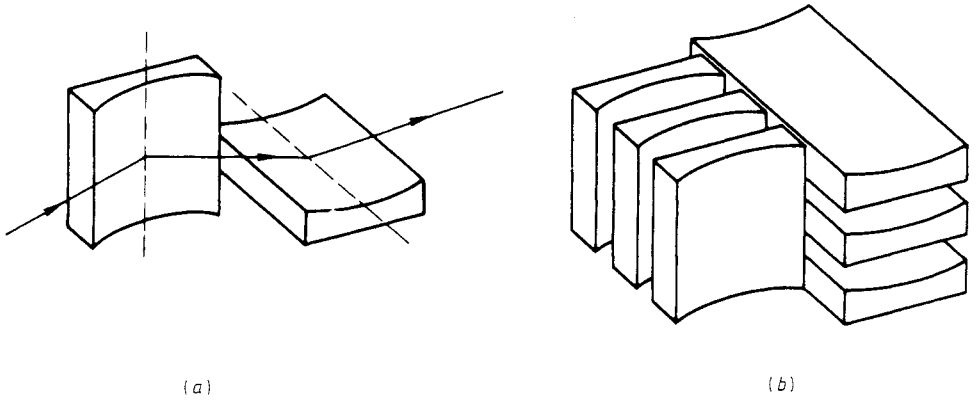

Figure 13. Schematic of the Kirkpatrick-Baez telescope. (*a*) shows a two-mirror combination, (*b*) displays a stack of several mirrors to increase collecting area.

4.1.3. Focusing collimator and 'lobster-eye' telescopes. The Wolter as well as the Kirkpatrick-Baez systems have in common a relatively narrow field of view which is practically limited to the grazing angle employed on the individual mirrors. Imaging systems of substantially larger field of view but of reduced angular resolution have been proposed by Schmidt (1975) and Angel (1979). The principal layout of Schmidt's design which he called a focusing collimator is shown in figure 14. The upper as well as the lower stack consists of a series of plane mirrors in an orthogonal configuration. Each mirror is furthermore assumed to be reflecting on both sides. The mirrors within each stack are arranged such that the envelope of the upper edges forms a section of a cylinder, so that the centre lines of the two cylinders are at a right angle, with their intersection point being the origin of the coordinate system. Each mirror plane is within the radial direction originating from the cylinder centre line of the corresponding stack. Therefore, each stack provides focusing in one dimension on a cylindrical surface located about halfway between the centre lines and the stack position. The focusing is not perfect because of the finite height of the mirror blades along the radial direction. In case of a one-dimensional device, i.e. only one stack, the field of view is restricted by that fraction of the cylinder circumference which is covered with mirrors. In principle, a field of 2π could be observed simultaneously.

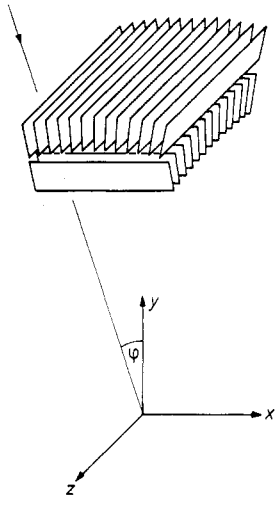

Figure 14. Flat mirror configuration of a two-dimensional focusing collimator (Schmidt 1975).

A variation of this design, which provides two-dimensional imaging, has been presented by Angel (1979). His device is composed of many small square-sided tubes with internal reflecting walls which are distributed over the surface of a sphere. The axis of each tube follows the radius vector of the sphere. This system looks like a honeycomb of rectangular cross section. If rays are reflected twice within one tube but from adjacent walls a two-dimensional image is formed on a spherical focal surface which has a radius half that of the sphere carrying the tubes. This type of optics is realised in the reflective eyes of lobsters and shrimps, giving the name to this particular type of x-ray telescope. That the optical principle is very similar to Schmidt's focusing collimator can be seen if the upper and lower stacks of his device are merged into one section forming square-sided tubes. In both designs there are rays passing through the optics with only one reflection or none at all. They appear as a diffuse or line-shaped background in the image. A realisation of this type of telescope would have great potential for continuous monitoring of large fields of view in the sky.

4.2. Examples of major telescopes

Grazing incidence telescopes have been built for more than two decades. While most of the systems have been of the Wolter type I, single paraboloids, Wolter type II and their Wolter–Schwarzschild equivalents, as well as one- and two-dimensional Kirkpatrick–Baez designs, have also been realised by various groups. A comprehensive review of this subject up to the beginning of the 1970s can be found, for example, in the paper by Underwood (1975). An account of the early history is given in the article by Giacconi *et al* (1981).

The development of telescopes reached a temporary culmination in 1973 when the solar S-054 (Vaiana *et al* 1977) and the S-056 (Underwood *et al* 1977) telescopes were flown aboard Skylab. One of the x-ray images of the Sun, which were taken with the S-054 telescope on film, is shown in figure 15. Since then further progress has been made, additional telescopes have been built and a second culmination point has been reached with the Einstein telescope which superseded all earlier devices in angular resolution and size. Additional telescopes specifically made for very high angular

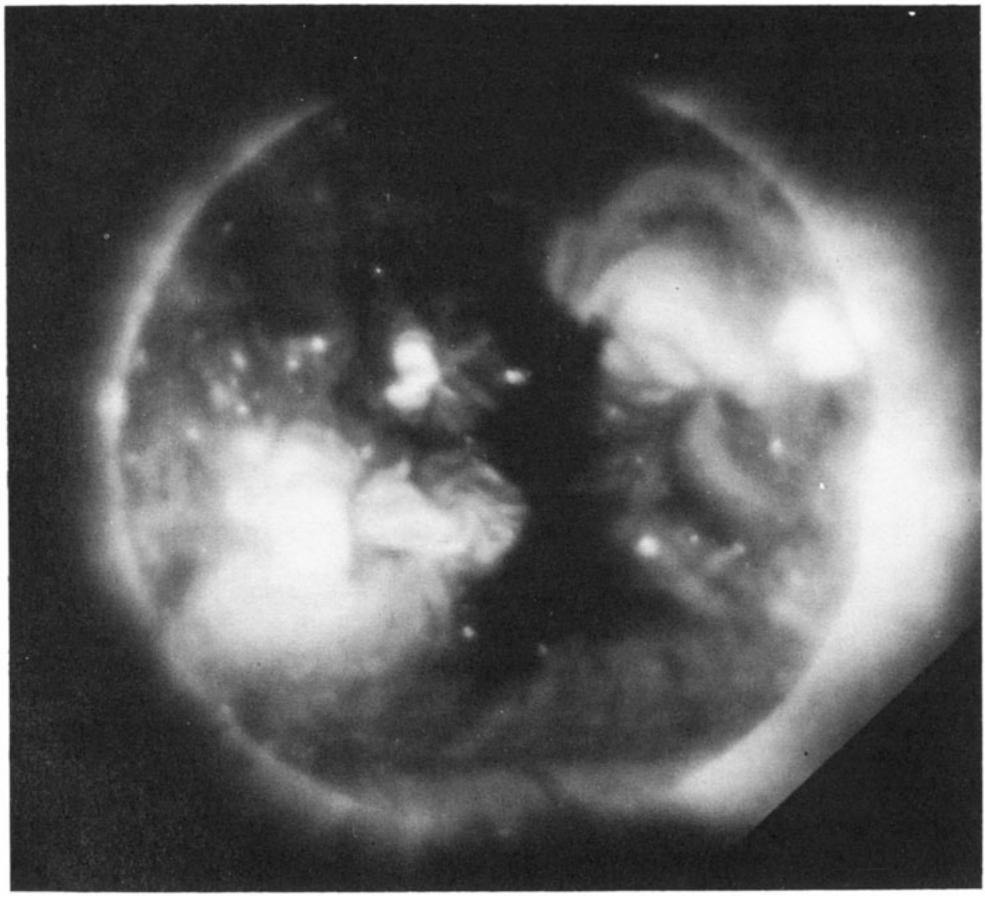

Figure 15. X-ray image of the 1 June 1973 Sun taken with the S-054 telescope aboard Skylab in the bands 2–32 Å and 44–54 Å. (Photograph courtesy of G S Vaiana, Harvard/Smithsonian Center for Astrophysics and the University of Palermo.)

resolution are now under development and large arrays of telescopes of small size and moderate resolution are also being studied. In the following a brief summary of existing or planned observatory telescopes is presented.

4.2.1. The Einstein observatory. The US Einstein observatory was launched into near-Earth orbit in November 1978 and was in operation till April 1981. The satellite carried the largest telescope placed into orbit so far. The high-resolution mirror assembly was of the Wolter type I with four nested shells. The aperture diameter of the largest paraboloid was 58 cm, while each of the paraboloids and hyperboloids was 51 cm long. The focal length was 345 cm. The mirrors were made from fused silica coated evaporatively with a thin nickel layer. The focal plane instrumentation consisted of a turret carrying four different detector systems which could selectively be commanded into the focus. The imaging detectors included a high-resolution imager (HRI) based on a channel plate device capable of 3 arcsec FWHM resolution and an imaging proportional counter of higher efficiency. Spectroscopy was possible with a solid-stage spectrometer

and the focal plane crystal spectrometer. In addition, an objective transmission grating could be used in conjunction with the HRI. Outside the focal plane of the telescope a collimated proportional counter was installed. A full description of the observatory is given by Giacconi *et al* (1979, 1981).

The Einstein observatory was commanded from the ground to point towards preselected objects or celestial fields. According to the latest edition of the Einstein (HEAO-2) observing catalogue a total of 5655 observations have been carried out (Seward and Macdonald 1983). In this way a few per cent of the complete sky area has been observed. High-resolution images of two young galactic supernova remnants, i.e. Cassiopeia-A and the Crab Nebula, are shown in figures 16 and 17, respectively.

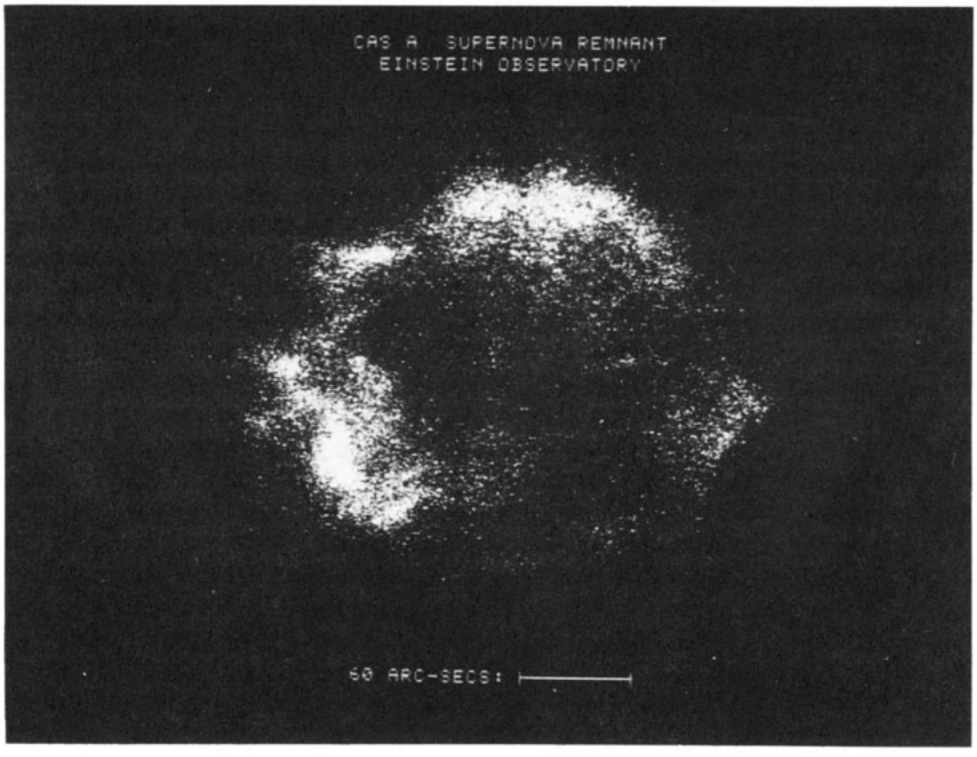

Figure 16. X-ray image of the galactic supernova remnant Cassiopeia-A taken with the Einstein observatory telescope and the HRI in focus. (Photograph courtesy of S. Murray, Harvard/Smithsonian Center for Astrophysics.)

4.2.2. The Salyut-7 RT-4M telescope. The Soviet Salyut-7 orbital station carries several experiments for x-ray astronomy. The RT-4M instrument is a grazing incidence telescope with a non-imaging flow gas proportional counter as the focal plane detector. The telescope is a two-fold nested Wolter type I design with a maximum entrance aperture 24 cm wide, a total mirror length of 48 cm and a focal length of 66 cm. The reflecting surfaces are coated with gold (outer telescope) and nickel (inner telescope) to provide an operating wavelength band between 44–100 Å over a field of view of 45′ by 3°. The detector entrance aperture is divided into three parallel sectors, viewing different fields (Mandelstam *et al* 1983).

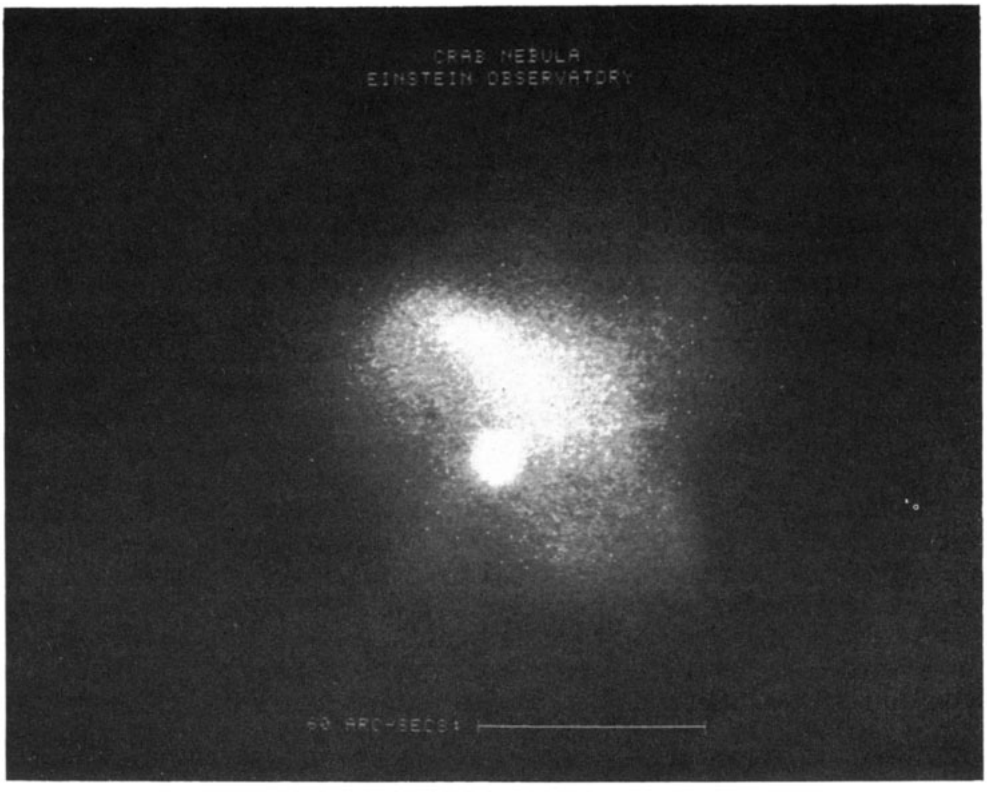

Figure 17. Einstein observatory HRI image of the Crab Nebula and the Crab Pulsar, the latter being the point-like source in the centre. (Photograph courtesy of F R Harnden Jr, Harvard/Smithsonian Center for Astrophysics.)

4.2.3. The Exosat observatory. The European Exosat satellite was launched in May 1983 and has been in operation since then. The orbit had been chosen to be highly eccentric with an apogee height of 200 000 km. Because of this high apogee uninterrupted pointing observation of a selected celestial field of up to 80 h is possible. The instrumental payload consists of the medium-energy experiment which is an array of collimated proportional counters, the gas scintillation proportional counter which features a spectral resolution better than a factor of two, and the low-energy experiment of two identical grazing incidence telescopes (Taylor *et al* 1981).

Each telescope is a two-fold nested Wolter type I system with a maximum entrance diameter of 28 cm and a focal length of 109 cm. Both paraboloid and hyperboloid have a length of 20 cm. The mirrors have been made by replication from a glass master. The reflective coating is gold, allowing measurements in the spectral band longward ~6 Å. Each focal plane is equipped with a position-sensitive detector (proportional counter) with spectral and spatial resolution capability and a channel multiplier array (CHA) which can provide spatial information only. A filter wheel in front of the detectors carries a variety of thin-film absorption filters with which broad band photometry can be made. Spectroscopy is enabled by two transmission gratings, one per telescope, which can be moved into the x-ray beam converging from the hyperboloids (de Korte *et al* 1981a, b). Figure 18 shows the high-resolution image of Puppis-A which is a galactic supernova remnant about 5000 yr old.

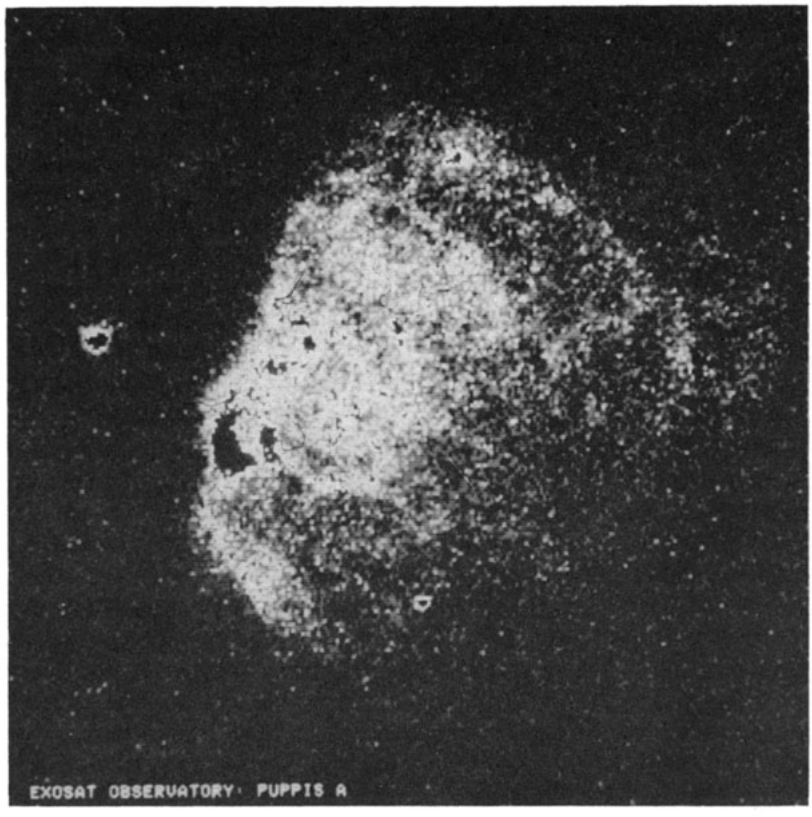

Figure 18. High-resolution x-ray image of the galactic supernova remnant Puppis-A as seen by the LE telescope and the CMA detector aboard the Exosat observatory. The vertical extent of the remnant in the image plane is 50 arcmin.

4.2.4. Rosat. The German x-ray astronomy satellite Rosat (Röntgensatellit) is planned to be launched in the second half of 1987 by the Space Shuttle in a circular low Earth orbit. The scientific payload consists of a large x-ray telescope covering the wavelength band from 6–100 Å and a wide field camera (WFC) from the United Kingdom, which is sensitive in the 60–300 Å region. The primary scientific objective of this mission is to perform the first all-sky survey with an x-ray imaging telescope leading to an improvement in sensitivity by several orders of magnitude compared with previous surveys. Based on the number flux relation for cosmic x-ray sources obtained from earlier missions, more than 10^5 sources are expected to be detected and located to better than 1 arcmin. Since the two telescopes are looking in parallel, spectral information about each source detected will be available from 6–300 Å simultaneously. After completion of the survey which will take about six months the telescopes will be operated in pointing mode performing detailed studies of selected sources with respect to spatial structures, spectral and time variability (Trümper 1984).

The x-ray telescope is a four-fold nested Wolter type I system with an aperture of 83 cm and a focal length of 240 cm. Each of the paraboloids and hyperboloids is 50 cm in length. The reflective coating is gold on the Zerodur-made mirrors. The on-axis resolution of the mirror assembly is specified to 5 arcsec (Aschenbach *et al* 1983). A prototype of the second outermost mirror system of 70 cm aperture has been completed.

A carousel carries three different imaging detectors out of which one at a time can be rotated into the focus. There are two redundant position-sensitive proportional counters (PSPC) (Pfeffermann and Briel 1983) and a high-resolution imager which is a copy of the instrument successfully flown on the Einstein observatory. The survey will be made with a PSPC in focus.

The WFC utilises a three-fold nested Wolter-Schwarschild type I design with an aperture of 58 cm, a total mirror length of 20 cm and a focal length of 53 cm. The field of view is circular and 5°. The resolution is 1 arcmin for on-axis rays and 2 arcmin radius averaged over the field of view. The mirrors are made from aluminium with the primary and secondary made out of one piece, whose internal surfaces are coated with gold. The focal plane assembly houses two identical XUV sensitised multi-channel plate detectors in front of which thin-film absorption filters provide three different wavelength pass bands (Willingale 1982).

4.2.5. The EUV Explorer. The American Explorer satellite programme includes an extreme ultraviolet astronomy telescope experiment (EUVE), which is expected to be launched 1987/88. The satellite is designed as a spinning spacecraft carrying four grazing incidence telescopes. Three telescopes are mounted perpendicular to the spin axis, thereby scanning the sky, whereas one telescope is pointed by viewing along the spin axis. The scanning telescopes will perform a full sky survey in about half a year and the pointing telescope will make deep exposures of a limited field of the sky. Each telescope is equipped with a channel plate detector including a dedicated fixed thin-film passband absorption filter. The telescopes are of an unnested Wolter-Schwarzschild type I design with a focal length of 50 cm. A prototype optic has been built with the primary and secondary machined in one piece. The aperture of the telescope is about 40 cm and the total mirror is 28 cm long. The resolution is specified to about 1 arcmin. A total field of view of 5° is feasible. This instrument will make observations in the EUV spectral range from 100–1000 Å (Bowyer 1983, Malina *et al* 1980) like the WFC on Rosat.

4.2.6. AXAF. The US Advanced x-ray Astrophysics Facility (AXAF) will carry the largest x-ray grazing incidence telescope planned so far. It will include a six-fold nested Wolter type I mirror assembly with an aperture of 1.2 m and a focal length of 10 m. The total length of the observatory is 13 m and it has a diameter of 4.5 m. The on-axis resolution is specified to 0.5 arcsec. The spectral coverage is from 0.1–10 keV. The grazing incidence angles range from 0.45–0.85°, allowing a total field of view of 1°. A variety of different instruments can be mounted into the focal plane assembly including imaging detectors of high spatial resolution, instruments of moderate spatial resolution but of high quantum efficiency and moderate spectral resolution and various spectrometers. Also, polarimetry with high sensitivity may be possible. AXAF is expected to be launched by the Space Shuttle in 1990 and is currently conceived to be revisited for maintenance and on-board servicing by the Shuttle on a regular basis (Zombeck 1983b).

4.2.7. LAMAR and XMM. The development of x-ray telescopes for the missions described above has aimed at the building of high angular resolution systems using one single instrument. Although the principle of nesting is being used frequently the total collecting area is, of course, limited by the maximum aperture feasible. To increase the collecting power the concept of using several telescopes in parallel has been

developed. In the United States this type of facility is being studied under the name LAMAR (large modular array of reflectors). Each module consists of a relatively small grazing incidence telescope and focal plane detector of moderate angular resolution. Many identical modules are packaged side by side providing the large area needed. For x-ray optics Kirkpatrick-Baez systems (Gorenstein 1979) as well as Wolter type I systems (Catura *et al* 1979) have been proposed.

In Europe a similar concept named XMM (x-ray multi-mirror mission) is being studied (Bleeker *et al* 1983). The model payload is based on a low-energy module for the energy region between 0.1-2 keV with a resolution capability of 10 arcsec and a high-energy module with spectral coverage up to 10 keV and 30 arcsec resolution.

5. Realisation of grazing incidence telescopes

5.1. Design

The properties of a grazing incidence telescope are described by its collecting area, efficiency, angular resolution and field of view. The collecting area is the geometric projection of the primary surface onto the entrance aperture and is more precisely called the geometric collecting area. The efficiency is the product of the reflectivities of the primary and the secondary (in the case of a two-mirror system) averaged over the grazing incidence angles present. Since reflectivity is highly wavelength-dependent so is the efficiency. The product of geometric collecting area times efficiency is often called the effective collecting area.

In order to describe the angular resolution one or more of a number of different terms are used. The point spread function (PSF) is the two-dimensional image intensity distribution of an infinitely distant point-like source. The line spread function (LSF) is the one-dimensional integral of the PSF. The edge spread function describes the response of the optics to an infinitely sharp and straight edge. The encircled energy function (EEF) is the outwards integration of the PSF over the radial coordinate. It describes the energy content within a circular area centred on the peak of the PSF as a function of image radius. Finally, the modulation transfer function (MTF) is also used, which is the Fourier transform of the PSF. To facilitate a brief characterisation very often only one number for the angular resolution is given, which is the full width at half-maximum (FWHM) of either the PSF or LSF. However, in astronomical applications very low photon fluxes are encountered and recorded with a noisy detector. Therefore, the signal-to-noise ratio should be maximised and the EEF should be as narrow as possible. In this context the half-energy radius (HER), which is the image radius containing half of the reflected photons, is a useful quantity. The PSF, like the other functions, is wavelength-dependent because of the mirror surface scattering. It should be noted that the PSF for on-axis rays is primarily determined by the fabrication and alignment of the mirrors, and not by the design. For off-axis rays geometric aberrations relevant to the particular telescope design take over, and the useful field of view is eventually terminated by the amount of image blur that can be tolerated.

The design of the mirror geometry of a particular telescope is usually obtained from ray tracing studies which take into account the physical constraints imposed by the volume and mass available from the launcher. Other constraints are due to the limitations of the machines to be used for fabrication. The choice of the type of telescope is influenced by the scientific requirements. Wolter type I designs are

preferred in survey experiments for which the optimisation criterion is the maximum effective collecting area times field of view. Sufficient angular resolution over the field of view is important since it allows to use small spatial image elements, the size of which determine the background count rate and thereby the signal-to-noise ratio of the instrument. Type II systems of comparable dimensions have larger aberrations due to field curvature which reduces the useful field of view. However, the type II systems feature much longer focal lengths and are therefore the optimum choice for dispersive spectroscopy applications.

The improvements in angular resolution which are offered by the Wolter-Schwarzschild configurations due to the suppression of coma are strongly dependent on grazing angle. The grazing angles of the telescope, on the other hand, are determined by the maximum photon energy for which the telescope has to have a reasonable effective collecting area. The design of the Rosat telescope was dictated by the requirement to have maximum sensitivity in the 0.5-2 keV band (Aschenbach *et al* 1983). The AXAF was designed to cover the energy range up to about 7 keV (Zombeck 1983a, b, c). In these designs the grazing angles are small and the difference in performance between the Wolter and Wolter-Schwarzschild designs is negligible. For wavelengths longer than ~50 Å the grazing angles can be made much larger and therefore the Wolter-Schwarzschild systems are preferred for EUV and XUV telescopes (Malina *et al* 1980, Willingale 1982). Van Speybroeck and Chase (1972) and Chase and Van Speybroeck (1973) give an empirical relation found by ray tracing calculations between blur circle radius, grazing angle, axial length of the primary and field angle. The angular resolution in terms of the blur circle radius as a function of field angle is shown in figures 19 and 20 for the Rosat x-ray telescope and the Rosat XUV wide field camera, respectively. Both figures illustrate the rapid increase of the aberration with increasing field angle which is clearly more pronounced for the x-ray telescope. The optimum focal surface for any grazing incidence telescope is not flat but curved towards the mirror system. A factor of typically two in angular resolution can be gained if the

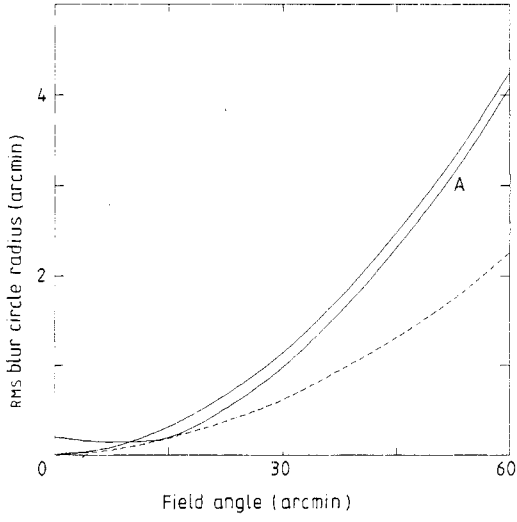

Figure 19. RMS blur circle radius plotted against field angle for the Rosat x-ray telescope on an optimally curved focal surface (----), a flat focal plane (——), and a flat focal plane shifted by 1 mm towards the mirror (A).

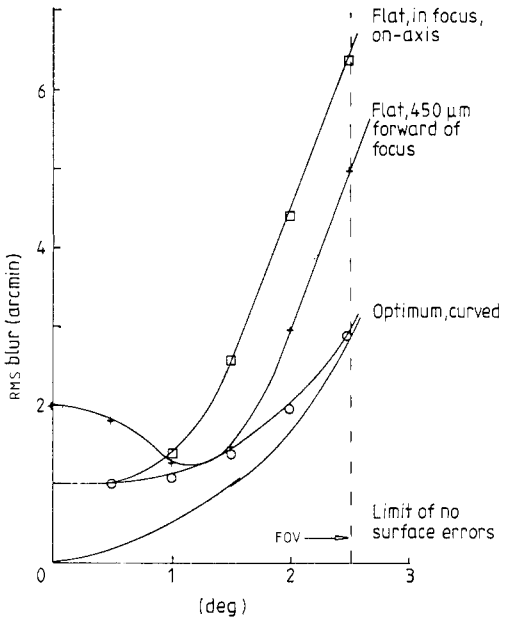

Figure 20. RMS blur circle radius plotted against field angle for the Rosat wide field camera. The lowest curve shows the relation for a perfect mirror system on the optimal focal surface, which is curved, out to the edge of the field of view (FOV). The remaining curves include 1 arcmin RMS mirror surface errors (Willingale 1982).

detector can be shaped to conform with the optimum focal surface. If a flat detector is to be used a more uniform blur across the field can be achieved by shifting the detector out of focus. However, the on-axis resolution is degraded.

The axial length L of the primary has an impact on both the collecting area and the off-axis angular resolution. Obviously the collecting area increases proportionally with L but the angular resolution becomes worse with increasing L, making a trade-off between angular resolution and collecting area necessary. Telescopes requiring only a narrow field of view can have very long primaries whereas for wide field survey telescopes, for example, an optimum L exists which is found by ray tracing.

Not only resolution but also the effective collecting area of a telescope varies with field angle. The latter is due to vignetting and to a change in reflectivity. Figures 21 and 22 show the effective collecting area plotted against photon energy at various off-axis angles for the Einstein (Van Speybroeck 1979) and Rosat mirror assembly, respectively. The shape of the curves is determined by the reflectivity of the coating material. The Einstein mirrors were coated with nickel and the dip at about 1 keV is due to the nickel L absorption edge. The coating of the Rosat mirrors is gold and correspondingly the dips occur at the O and N absorption edges. The M absorption edges lead to the cut-off in collecting area above ~2.2 keV. Both figures are the result of calculations using the reflection off perfect mirrors surfaces as described in § 2. Due to the wider aperture and the larger grazing angles of the Rosat mirrors the collecting area is substantially larger at low energies compared with the Einstein telescope.

In the case of a prime focal plane detector the design of the mirror system is influenced by the product of the effective collecting area times detector efficiency which has its own energy dependence. In the case of Rosat the prime detector is a thin-window

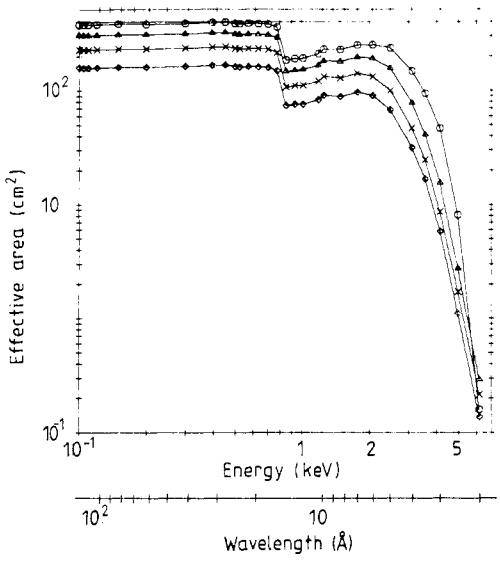

Figure 21. Theoretical effective collecting area of the Einstein mirror assembly at four different field angles: ○, zero; △, 20 arcmin; ×, 30 arcmin; ◇, 40 arcmin. Surface scattering losses and obstruction by support elements are not included (Van Speybroeck 1979).

proportional counter. The theoretical effective area of the complete instrument is shown in figure 23. The shape of the response curve is now dominated by the jump at 0.28 keV, which is due to the carbon K absorption edge of the detector window material.

5.2. Fabrication

The building of a telescope includes the fabrication of the x-ray mirror shells, the assembly of the mirrors and the mounting of the complete assembly into a telescope structure. For the fabrication of the mirror elements two different methods have been used: the conventional direct grinding and polishing of the mirror substrate and the replication from a highly polished master. Quite recently a third possibility was studied. The Wolter type I paraboloids and hyperboloids have been replaced by straight cones, which for short mirror segment length, small grazing angles and long focal length are a reasonable approximation which can lead to an angular resolution of 0.5 arcmin HER. A prototype of such a mirror system has been built by Serlemitsos (1981) by using high quality but commercially available aluminium foil ~125 μm thick, which was overcoated with 10 μm acrylic lacquer to produce a smooth surface. Finally, a layer of ~500 Å of gold was vacuum-deposited on top. Reflection measurements gave satisfactory results. An angular resolution of 3 arcmin HER was measured independent of energy (1.2 keV $\leq E \leq$ 10 keV), a result which indicates that assembly errors may have been primarily the source for the relatively large HER value.

The replication technique has been applied with great success in the Exosat programme. The replication process is described in detail by Lainé *et al* (1979). Figure 24 shows the principle of the manufacturing sequence. A master mandrel of glass—BK7 in the case of Exosat—with a highly polished surface is made in the negative shape of the required x-ray mirror. The mirror substrate was made from beryllium. The 3.5 mm thick shells were turned on a high precision lathe to the approximate shape

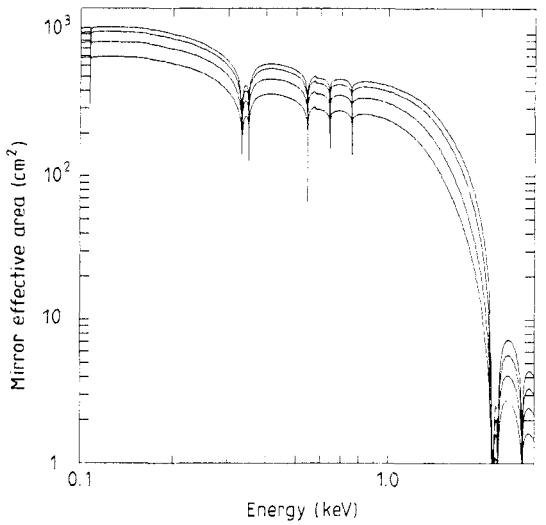

Figure 22. Theoretical effective collecting area for the Rosat x-ray mirror assembly at field angles 0, 20, 40 and 60 arcmin to be read for each curve from top to bottom. Surface scattering losses are not included, but obstruction by support elements has been taken into account.

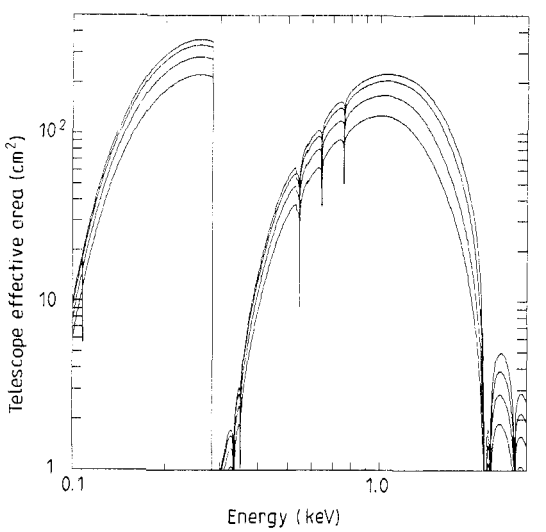

Figure 23. Theoretical effective collecting area of the Rosat x-ray telescope including the efficiency of a 1 μm thin-window proportional counter. Mirror data and field angles are as in figure 22.

(to within a few microns) of the desired paraboloid or hyperboloid. The gold-coated mandrel is placed onto the mirror substrate with a thin epoxy layer separating the two surfaces. After the curing of the epoxy the mandrel is extracted leaving the gold layer moulded into the x-ray mirror. After cleaning the mandrel can be used for further production. Measurements of the profile and x-ray scattering tests showed that the quality of the replica mirror is very close to that of the original master. By this technique it was possible to produce extremely lightweight (7 kg) mirror assemblies.

The application of a replication technique has also been reported by Hunter *et al* (1980) and Hudec and Valníček (1984), who manufactured the mirrors for the RT-4M

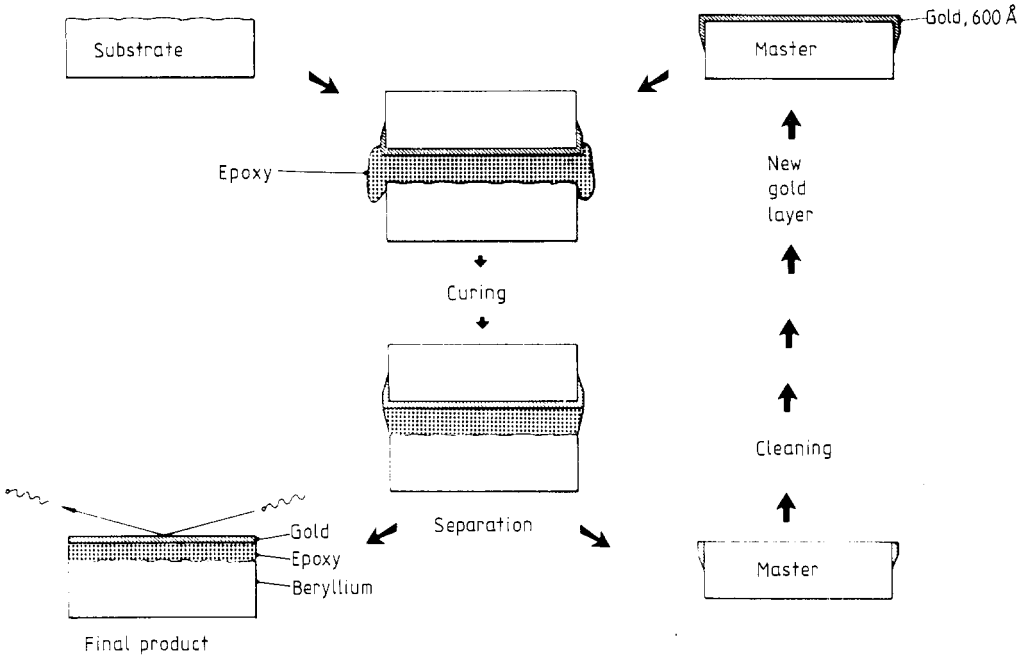

Figure 24. Sequence of replication techniques used for the Exosat telescopes (Lainé *et al* 1979).

telescope aboard the Salyut-7 orbital station, and quite recently by Ulmer *et al* (1984). The latter two groups used electroforming to produce the mirror on the polished mandrel surface.

The traditional way of producing optics is by grinding and polishing the mirror substrate directly. In this case the working sequence proceeds as follows. The first step is to produce the mirror blanks. For the Einstein mirrors fused quartz was selected as the mirror carrier material and the mirror blanks were made by fusing barrel-stave-shaped elements in a centrifuge (Giacconi *et al* 1981). The Rosat mirror blanks have been produced from solid Zerodur blocks out of which the conical mirror shells have been drilled. Normally, the blanks have to undergo stress relief processes. In the case of metal mirrors this is done by aging, whereas vitreous materials are polished on the outer surface. The next step is the figuring of the contour of the inner surface. Depending on the resolution requirement different types of machines may be used. For low resolution mirrors it is sufficient to use a simple numerically controlled lathe. For mirrors with higher resolution requirements dedicated high-precision grinding machines have to be used. The method of loose abrasive grinding proved to be very successful in the case of the Einstein and Rosat mirrors. In the case of Rosat, the mirrors are placed vertically on an air-bearing table and the inner contour is produced by means of a grinding wheel. However, the forces which have to be exerted on the surface are rather high, so that the mirror would react by deforming, if it were not supported. The Rosat mirror cones are embedded into a conical aluminium structure as shown in figure 25. The mirror is fixed by several hundred pins which are positioned in the corresponding holes in the support structure during mounting. It is essential that the mirror shell is completely relaxed so that it settles with its force-free shape.

Figure 25. Mounting of a Rosat Zerodur mirror shell into its aluminium support structure necessary for grinding and polishing (photograph courtesy of Carl Zeiss).

The necessity of supporting the mirror during grinding is reduced if single-point diamond turning is used. Several diamond-turning facilities are now available which are capable of figuring mirrors of 1 m diameter and more (Wills-Moren 1982). Finish cuts of less than a micron for metal mirrors have been reported with cutting forces below 1 g (Donaldson *et al* 1981). An overview of the current status of high-precision machining can be found in volume 433 of the *Proceedings of the Society of Photo-Optical Instrumentation Engineers.* The major drawback of single-point machining is the rather high local slopes at short spatial wavelengths on the surface. For x-ray mirrors this requires subsequent polishing. After the grinding process the coarse figure of the x-ray mirror is fixed. The subsequent polishing provides the final figure and the smoothness necessary for x-ray quality.

Polishing of the Einstein as well as the Rosat mirrors has been done on a roller polishing machine. Figure 26 shows one of the Einstein mirrors during polishing. The mirror shell is supported by two belts on which the mirror is rotated to avoid any directional preference. The Rosat mirrors are polished still embedded in the outer support structure. The final figuring and polishing seems at present the most demanding step because of the high asphericity of x-ray mirrors. Several polishing tools of different size and structure are used to overcome this difficulty. A more detailed description of the working sequence in the fabrication of the Einstein mirrors can be found in the paper by Young (1979).

Since the performance of the mirrors cannot be measured with x-rays during the fabrication process, the x-ray optical requirements have to be translated into mechanical tolerances, which can be controlled by appropriate metrological devices. In principle, the performance of a mirror is determined by its two-dimensional macro- and micro-topography. However, to cope with the available metrology methods the errors are

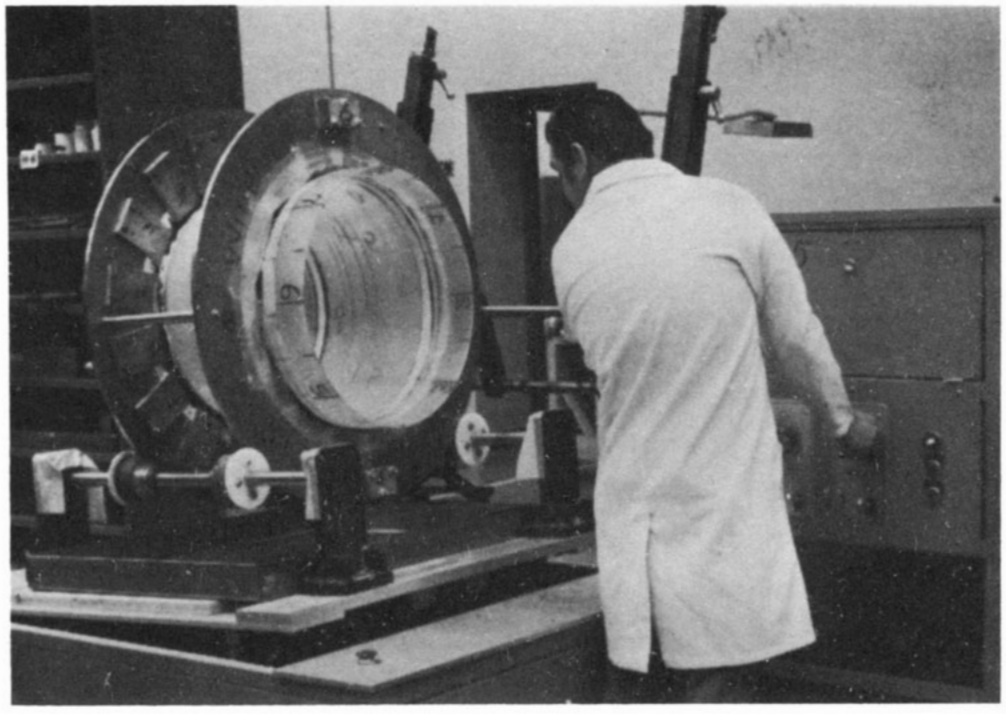

Figure 26. The largest hyperboloid of the Einstein mirror assembly on the roller polishing machine at Perkin Elmer (Young 1979).

broken down into one-dimensional distortions. A discussion of the various possible mechanical deformations of a conicoid can be found in the paper by Zombeck (1981). Experience shows that out of the 7 error sources listed only two are crucial during fabrication. The first is differential out of roundness, i.e. a variation of the circularity along the axial direction, which is equivalent to axial slope errors. The roundness of a workpiece may be measured on a high-precision air-bearing rotary table or directly on the grinding machine (Beckstette and Heynacher 1983). For the Einstein mirrors a differential out of roundness of 1 μm has been achieved on average with a minimum value of 0.5 μm (Young 1979). The Rosat mirror shells which have been completed also show values as low as 0.5 μm. The second important requirement is the accuracy of the meridional profile, which can also be expressed in terms of axial slope errors. In the case of the Rosat mirrors the profile is measured by means of a stylus instrument (Heynacher and Reinhardt 1979, Beckstette and Heynacher 1983). An inductive probe mounted on an air-bearing slide scans the profile difference between the mirror workpiece and a spherical master reference. A sample of a profile achieved on one of the Rosat prototype mirrors is shown in figure 27. The profile can be expanded in a Fourier series and the power spectral density can be used to determine the actual measurement noise level which appears at high frequencies (see figure 28). By cutting off the high-frequency terms the true profile and the average axial slope errors are determined. Values between 0.4–0.7 arcsec RMS have been obtained for the Rosat paraboloid flight mirrors. The Einstein mirrors showed 0.6 arcsec slope errors for 91.5% of the surface area averaged for 6 mirror elements (Young 1979). The Fourier representation of the profile is also useful for examining the mirror surface for the

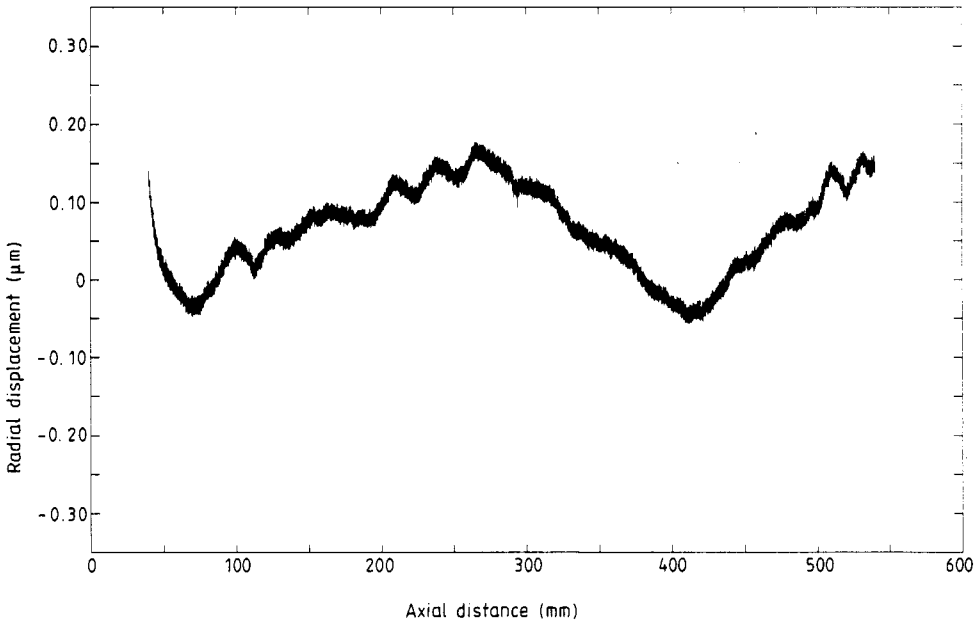

Figure 27. Meridional surface profile of a hyperboloid mirror of the Rosat prototype telescope as measured with a stylus instrument at Carl Zeiss. Short-scale wiggles are due to measurement noise.

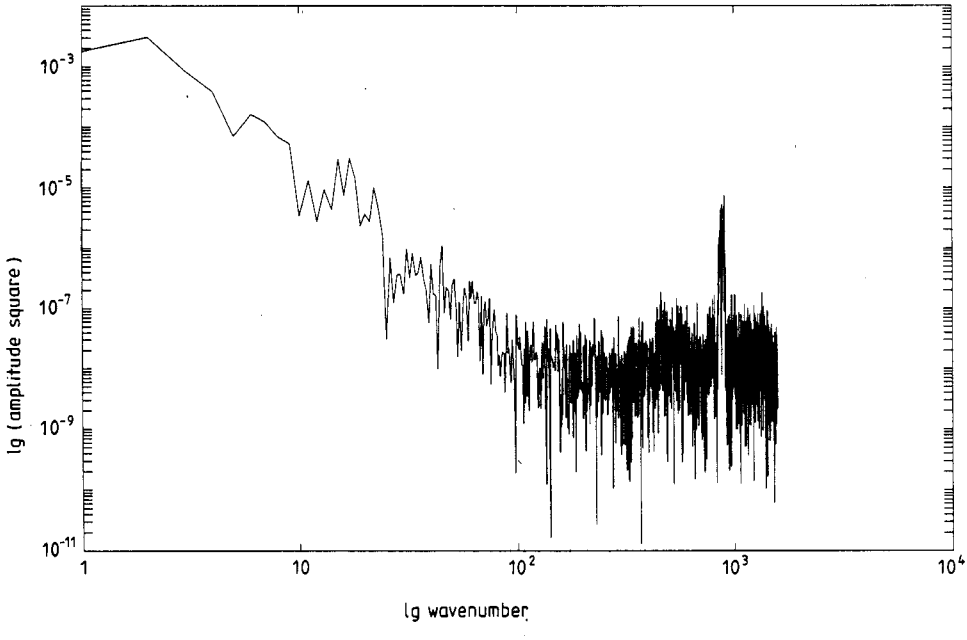

Figure 28. Fourier amplitude square spectrum of the mirror profile shown in figure 27. A wavenumber value of 1 corresponds to a spatial surface wavelength of 500 mm. For wavenumbers $\geqslant 100$ the spectrum is due to measurement noise including the peak at about a wavenumber of 900.

periodic patterns which are very likely to be introduced by the shape or motion of the polishing tool.

The extension of the meridional profile into the range of shorter spatial wavelengths leads into the microroughness regime which causes scattering. The scattering properties can be measured directly by means of x-rays, if the mirror can be transferred to an x-ray test facility. This has been done in the case of the mirrors of the MPI 32 cm telescopes which were made from aluminium and flown on sounding rockets (Trümper *et al* 1979). Figure 29 shows the angular scattering distributions as they improved from polishing step to polishing step. Eventually a RMS microroughness of 6.7 Å was achieved. For large mirrors and a tighter time schedule this cannot be done on a regular basis. In the case of the Einstein mirrors FECO interferometry (fringes of equal chromatic order) has been applied. Small size replicas from the mirror surface have been taken and compared with a reference flat (Ledger 1979). An average microroughness of 22 Å has been reported (Van Speybroeck 1977). More recently, optical heterodyne interferometry has been developed (Sommargren 1981). The surface of the mirror to be inspected is illuminated by two focused laser beams of slightly different frequencies and the reflected beams are brought to interference. The phase of the

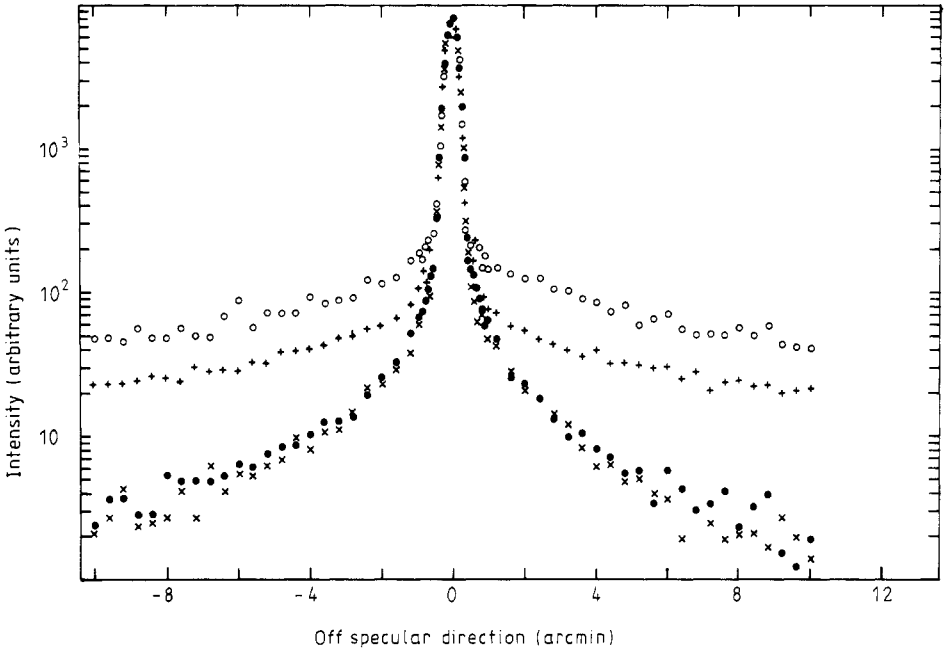

Figure 29. X-ray pencil beam measurements of the scattering distribution of the MPI 32 cm telescope after different polishing steps.

	Polishing steps	Scattering within 20 arcmin (%)	Microroughness (Å)
○	1	23.4	15.5
+	2	16.5	11.3
×	3	4.2	5.5
●	4	5.1	6.7

sinusoidal intensity modulation is related to the height difference between the two illuminated patches. By moving one of the beams across the surface the profile can be traced with a vertical resolution of a few ångströms. This type of system has been recently adapted to the Rosat mirror geometry and microroughness measurements have been carried out. Comparison with x-ray scattering measurements yielded satisfactory agreement between the two methods, averaged over the number of patches studied, in correlation length and microroughness level. Based on x-ray scattering results microroughness levels as low as 3.5 Å have been achieved on the first Rosat flight model mirrors.

The final step in the fabrication sequence is the coating of the inner mirror surface either by electroplating or by evaporation in a dedicated vacuum chamber. A typical thickness of the x-ray reflecting coating is ~500 Å on top of a chromium or some other binder film. Mathur *et al* (1979) describe the coating procedure of the Einstein mirrors in great detail.

The assembling of the individual mirrors can be carried out either in a vertical or horizontal configuration. For the Einstein mirrors the horizontal approach was taken which meant that the mirrors had to be supported by 32 calibrated forces to achieve a gravity-free state. For the assembling of the Rosat mirrors a dedicated alignment tower was erected so that the mirrors are mounted in vertical orientation. The distortion

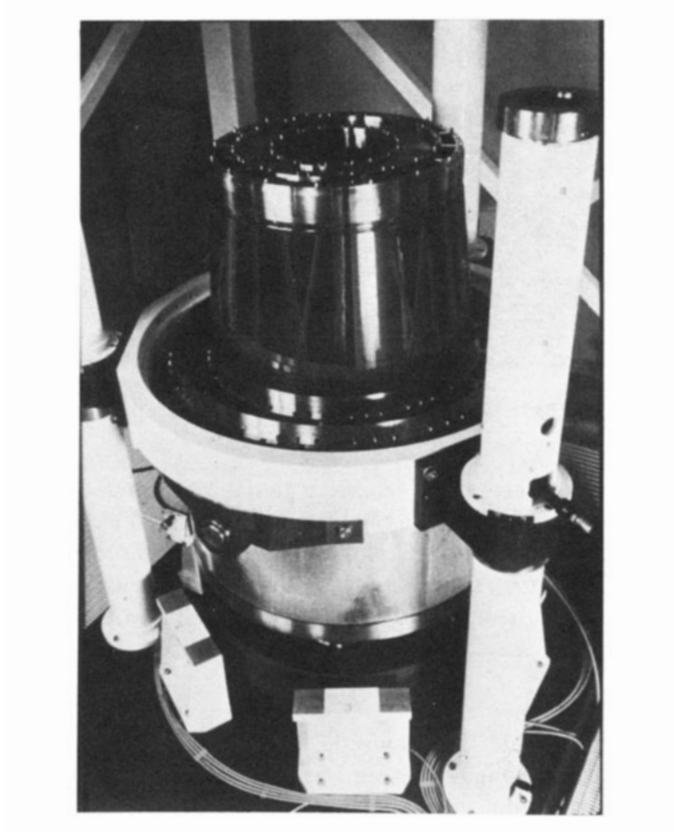

Figure 30. View of the assembled Rosat prototype mirror system. In the upper half of the photograph the hyperboloid with the exit and centre flanges can be seen; the 70 cm wide paraboloid is enclosed in the lower protection tube (photograph courtesy of Carl Zeiss).

of the mirrors due to gravity is very small in this case and no zero-g counterbalance has to be used. The alignment is done optically in either case by monitoring the optical focus with a microscope. For nested telescopes like the Einstein and Rosat telescopes the individual mirror shells are bonded to a massive Invar flange bridging the paraboloid/hyperboloid interface. Figure 30 shows details of the mounting process of the Rosat prototype telescope. Single-shell metal mirrors can be bolted together by means of dedicated flanges on the outer surface, if they had not been made out of one piece. Figure 31 shows as an example the MPI 32 cm telescope which was made out of four pieces of aluminium to ease polishing.

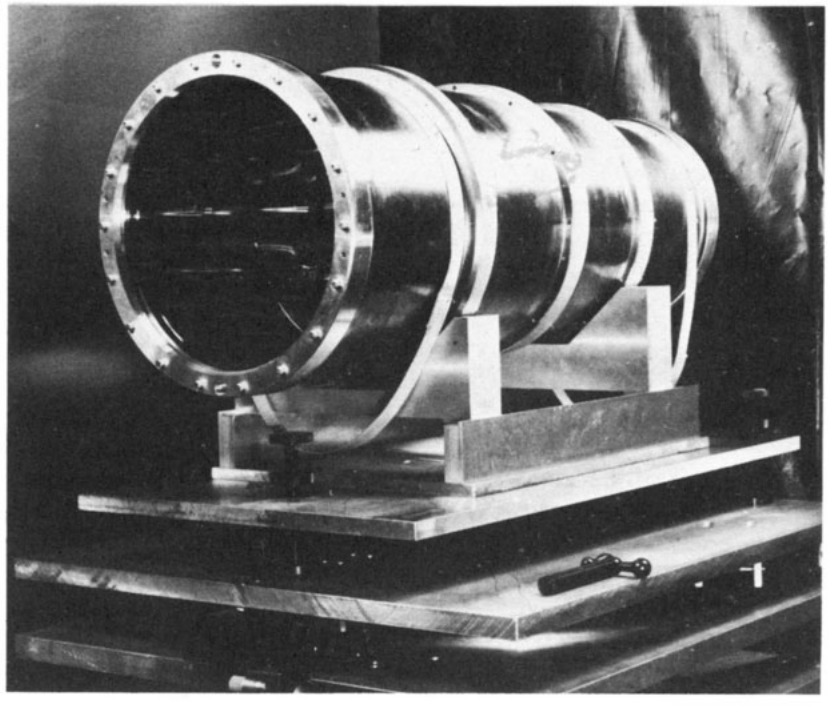

Figure 31. The MPI 32 cm aluminium telescope.

In the case of nested telescopes excessive radial vibrations of the mirrors at the front and rear end of the mirror assembly have to be damped by bonding an entrance and exit aperture flange to the mirrors. Figure 32 shows a photograph of the Einstein mirror assembly where the aperture flange with the four circular concentric entrance slits—one each for each mirror section—can be seen rather nicely.

5.3. Performance analysis

Very little data have been published about the actual performance of grazing incidence telescopes, in particular the angular resolution achieved. The few exceptions are listed in table 1 together with the specifications for the Rosat and AXAF telescopes. It is interesting to note that each of the telescopes shows a FWHM angular resolution of a few arcsec. It seems as if the FWHM resolution of a telescope is more related to the alignment than to the quality of the surfaces themselves. The half-energy radius (HER),

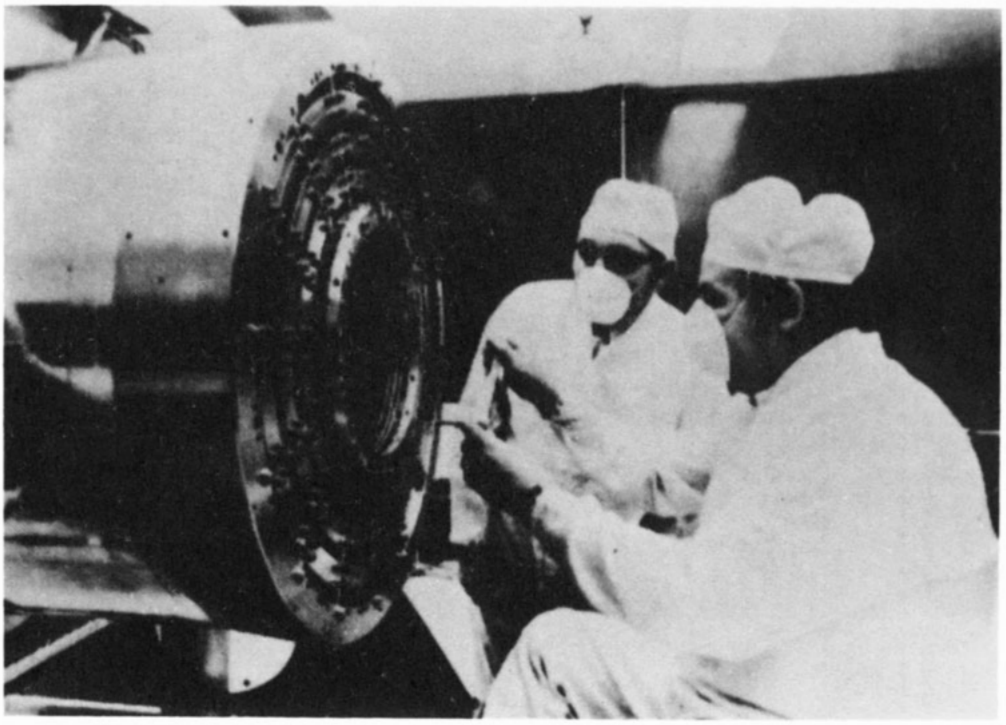

Figure 32. Entrance aperture view of the Einstein mirror assembly at Perkin Elmer (Van Speybroeck 1977).

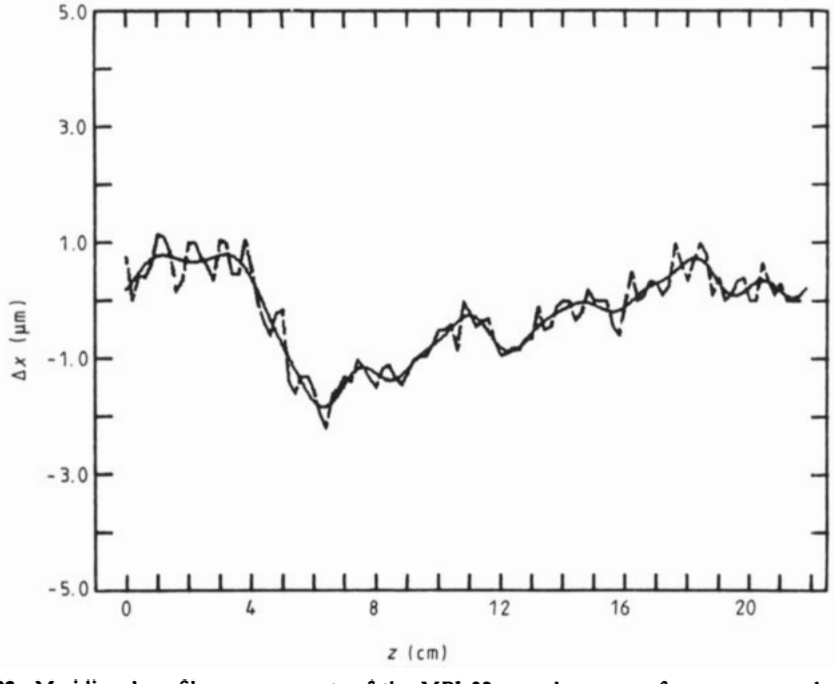

Figure 33. Meridional profile measurements of the MPI 32 cm telescope surface: - - -, raw data; ——, Fourier-smoothed data.

Table 1. Main characteristics of high-resolution x-ray telescopes.

Telescope (references)	Design parameters							On-axis angular resolution (arcsec)		
	Type	Materials	Focal length (mm)	Maximum diameter (mm)	Total mirror length (mm)	Geometric collecting area (cm^2)	Energy range (keV)	FWHM	HER‡ (44.8 Å)	HER (8.3 Å)
ATM S-054 (Vaiana *et al* 1977, Davis *et al* 1979)	Wolter I nested pair	Kanigen on beryllium	2130	304	342	42	0.2–6	4	18	48
ATM S-056 (Underwood *et al* 1977)	Wolter I single shell	Fused silica	1903	247	?	15	0.2–2	2	?	?
Einstein Observatory (Van Speybroeck 1979, Giacconi *et al* 1979)	Wolter I nest of 4 shells	Chrome/nickel on fused quartz	3440	580	1022	350	0.2–4	3	4	5
MPI (Trümper *et al* 1979, Aschenbach *et al* 1979)	Wolter I single shell	Kanigen on aluminium, evaporated gold surface	1427	322	810	106	0.1–2	6	26	37
Exosat qualification model (de Korte *et al* 1981a)	Wolter I nested pair	Gold clung to beryllium by epoxy layer	1090	278	400	89	0.04–2	5	10	20§
Rosat† (Trümper 1983, Aschenbach 1983)	Wolter I nest of 4 shells	Gold on Zerodur	2400	835	1000	1150	0.1–2	5	2.5	2.5
AXAF† (Zombeck 1983b)	Wolter I nest of 6 shells	Gold/nickel on quartz or Zerodur?	10 000	1200	1650	1500	0.1–10	0.5	0.5 at 5 Å	

† Specifications.

‡ HER (half-energy radius) is the radius of the circle containing half of the reflected energy.

§ The Exosat flight model shows a HER (8.3 Å) value of 15 arcsec (de Korte 1982).

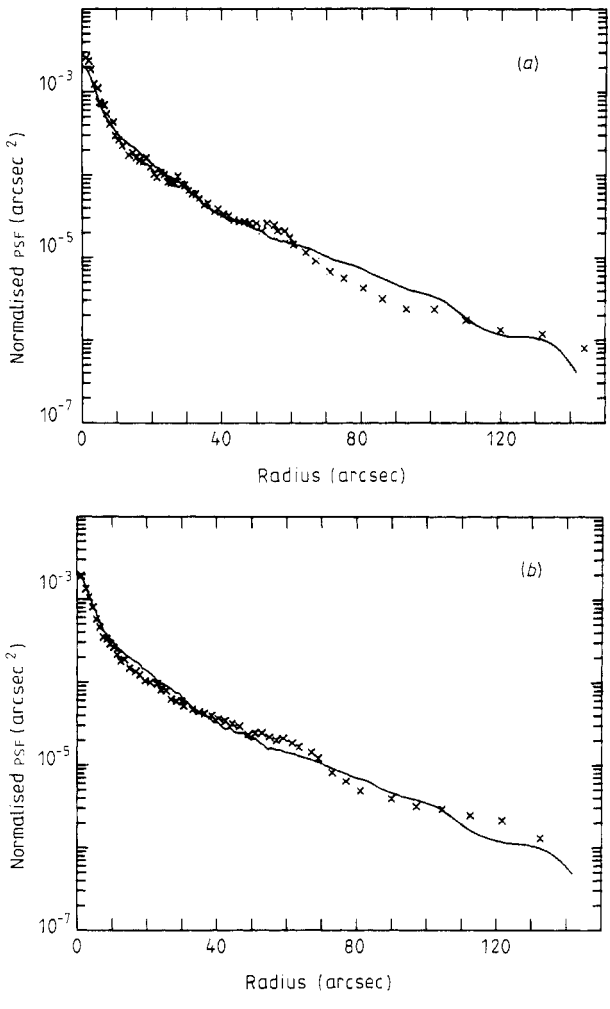

Figure 34. Comparison of measured (×) and theoretical (——) point spread functions of the MPI 32 cm telescope at $\lambda = 44.8$ Å (*a*) and $\lambda = 13.3$ Å (*b*).

which defines the radius of the circle containing 50% of the reflected intensity, is very different from telescope to telescope. For the S-054 telescope the HER value is strongly energy-dependent, indicating that microroughness scattering may be the origin. The HER value for the MPI 32 cm telescope is much less energy-dependent, making axial slope errors the most likely source. Figure 33 shows the data from one of 16 stylus meridional profile measurements. Subsequent Fourier analysis has been used to construct the noise-free profile. From the 16 cleaned profiles the axial slope distribution has been computed, resulting in a point spread function shown in figure 34 (Aschenbach *et al* 1980). The agreement between model and measurement over three orders of magnitude is remarkable and underlines the dominant contribution of axial slope errors, but also the geometric optics approach used in the calculation. Scattering theory in the Kirchhoff approximation has been used to incorporate microroughness scattering at a level of 6.2 Å which was derived from x-ray pencil beam tests. This accounts for the minor wavelength dependence, which is apparent in figures 34(*a*) and (*b*).

De Korte *et al* (1981a, b) have used first-order vector theory to predict the point spread function at 8.3 and 13.3 Å from measurements taken at 44 Å for the Exosat qualification mirror assembly. With a surface roughness of 19 Å and a correlation length of 20 μm they obtained an excellent agreement with the measurements as shown in figure 35.

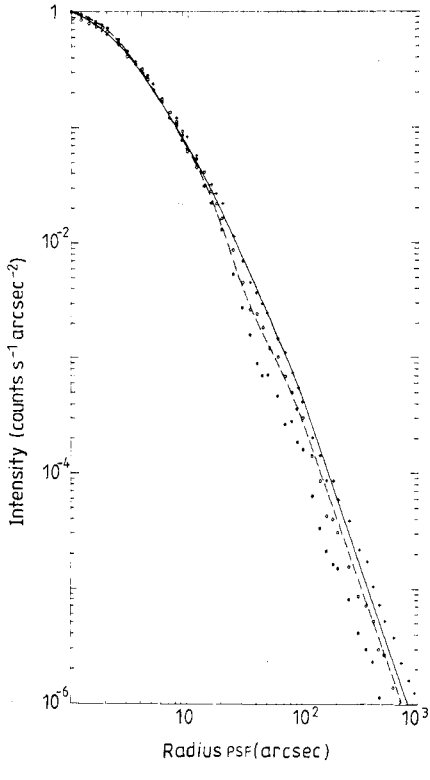

Figure 35. Point spread function of the Exosat qualification telescope (de Korte *et al* 1981b). Measured: ●, 44 Å; ○, 13.3 Å; +, 8.3 Å. Theory: - - -, 13.3 Å; ——, 8.3 Å.

The Einstein mirror assembly shows the lowest values for the HER out of the telescopes built so far. Van Speybroeck (1979) has attempted to model the point spread function including the individual error contributions from axial slope, out of roundness and microroughness scattering through the scalar theory. The comparison between model and data at three different photon energies for the encircled energy function is shown in figure 36, revealing a discrepancy which becomes more pronounced with increasing energy.

A key feature for improving the understanding of x-ray mirrors is to have the meridional profiles available over all spatial wavelength scales from the axial length of the mirror down to the sub-micron range. The metrology used so far has not given this kind of information. However, metrology has made substantial progress in recent years by means of mechanical scanning as well as of contact-free optical devices from which future telescope projects will benefit. Overviews of presently available metrology techniques can be found in the articles by Bennett (1980), Franks (1981), Price (1981), Stedman (1981), Zombeck *et al* (1982) and Williams *et al* (1984).

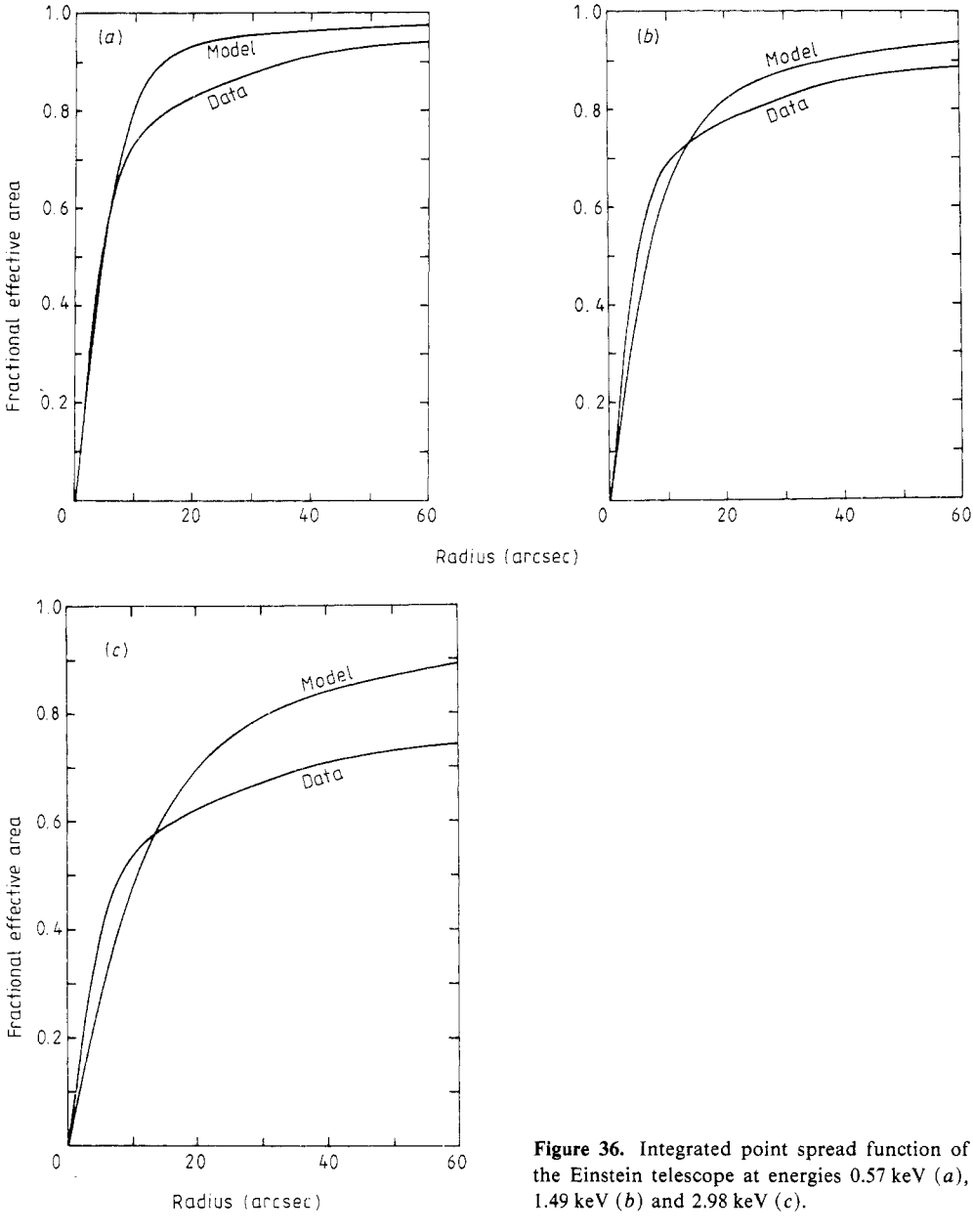

Figure 36. Integrated point spread function of the Einstein telescope at energies 0.57 keV (*a*), 1.49 keV (*b*) and 2.98 keV (*c*).

6. Conclusions

The past 20 years have seen great progress in the fabrication and application of grazing incidence telescopes. They have proved to be rather versatile instruments feeding a variety of imaging detectors and spectrometers in the same manner as their optical counterparts. Normal incidence reflectivity of available coatings drops quite rapidly for wavelengths shorter than ~800 Å, so that grazing incidence telescopes become the more efficient instruments and may be used not only in the traditional x-ray region

but throughout the spectrum from 15 eV to 10 keV, over almost three orders of magnitude in photon energy.

High-precision machining is now capable of producing finish cuts to an accuracy of a fraction of a micron. Use of on-line metrology during machining and polishing should be supported in order to shorten production timescales.

The polishing techniques have advanced to such a degree that flat samples with microroughness levels as low as 2 Å have been produced. The transfer of the technique from flat samples to highly aspherical telescope mirrors has been demonstrated successfully at least to roughness levels of 20 Å while simultaneously maintaining the figure. The transfer to even lower levels is currently pursued in the Rosat mirror fabrication with roughness levels as low as 3.5 Å being demonstrated. The AXAF development is expected to produce even finer mirrors.

The replica technique as used for the Exosat mirrors has produced excellent results and seems to be well suited to producing the large number of telescopes of moderate angular resolution required for a LAMAR or XMM type facility.

Independent of any particular applications and despite the fact that excellent telescopes have been built, there is a need for experimental and theoretical work in order to better understand the reflection and scattering of x-rays from real mirrors with rough surfaces. This includes systematic x-ray measurements of reflectivity and scattering of samples of graded microroughness accompanied by other topographic measurements to identify the impact of surface geometry. Scattering theories are to be developed which are not restricted to smooth surfaces and which can cover the entire band of spatial surface frequencies from the sample size to the sub-micron range. Finally, they should explain the observed reduction in reflectivity with increasing scattering level.

References

Angel J R P 1979 *Astrophys. J.* **233** 364

Aschenbach B and Bräuninger H 1978 *Japan. J. Appl. Phys.* **17** *Suppl. 17-2* 323

Aschenbach B, Bräuninger H, Hasinger G and Trümper J 1980 *Proc. SPIE* **257** 223

Aschenbach B, Bräuninger H and Kettenring G 1983 *Adv. Space Res.* **2** No 4, 251

Aschenbach B, Bräuninger H, Ondrusch A and Predehl P 1981 *Proc. SPIE* **316** 175

Aschenbach B, Bräuninger H, Stephan K-H and Trümper J 1979 *Proc. SPIE* **184** 234

Barbee T W 1981 *Low Energy X-ray Diagnostics. AIP Conf. Proc. 75* ed D T Attwood and B L Henke (AIP: New York) p 131

Bass F G and Fuks I M 1979 *Wave Scattering from Rough Surfaces* (Oxford: Pergamon)

Beckmann P and Spizzichino A 1963 *The Scattering of Electromagnetic Waves from Rough Surfaces* (Oxford: Pergamon)

Beckstette K and Heynacher E 1983 *Proc. SPIE* **429** 126

Bennett H E 1980 *Opt. Engng* **19** 610

Bennett H E and Porteus J O 1961 *J. Opt. Soc. Am.* **51** 123

Bilderback D H 1981 *Proc. SPIE* **315** 90

Bleeker J, Culhane J L, Koch-Miramond L, Olthof H, Schnopper H W, Taylor B G and Whitcomb G P 1983 *XMM—X-ray Multi Mirror Assessment Study. ESA Rep.* SCI(83)2

Bol Raap B E, Le Poole J B, Dijkstra J H, de Graaf W and Lantwaard L J 1969 *Small Rocket Instrumentation Techniques* ed Ken-Ichi Maeda (Amsterdam: North-Holland) p 203

Bowyer S 1983 *Adv. Space Res.* **2** No 4, 157

Bräuninger H, Einighammer H J, Feitzinger J V, Fink H H, Höhn D H, Koops H, Krämer G, Mayer U, Möllenstedt G and Mozer M 1971 *Solar Phys.* **24** 395

Burnight T R 1949 *Phys. Rev.* **76** 165

Buteux R H 1953 *J. Opt. Soc. Am.* **43** 618
Cash W, Sheeley D L and Underwood J H 1979 *Proc. SPIE* **184** 228
Catura R C, Brown W A and Acton L W 1979 *Proc. SPIE* **184** 73
Catura R C, Brown W A, Joki E G and Nobles R A 1983 *Opt. Engng* **22** 140
Chase R C and Van Speybroeck L P 1973 *Appl. Opt.* **12** 1042
Chubb T A, Friedman H, Kreplin R W, Blake R L and Unzicker A E 1961 *Mém. R. Sci. Liège 5th ser.* **IV** 235
Church E L 1979 *Proc. SPIE* **184** 196
Church E L, Jenkinson H A and Zavada J M 1979 *Opt. Engng* **18** 125
Church E L and Zavada J M 1975 *Appl. Opt.* **14** 1788
Compton A H 1923 *Phil. Mag.* **45** 1121
Compton A H and Allison S K 1935 *X-rays in Theory and Experiment* (New York: Van Nostrand Reinhold)
Costa E, Auriemma G, Boccaccini L and Ubertini P 1978 *Appl. Opt.* **17** 621
Croce P and Névot L 1976 *Rev. Phys. Appl.* **11** 113
Croce P, Névot L and Pardo B 1972 *C. R. Acad. Sci., Paris* **274**
Daniels J, Festenberg C, Raether H and Zeppenfeld J 1970 *Springer Tracts in Modern Physics* **54** 77
Davis J M, Krieger A S, Silk J K and Chase R C 1979 *Proc. SPIE* **184** 96
de Korte P A J 1982 *New Techniques in X-ray and XUV Optics. Proc. RAL Symp.* ed B J Kent and B E Patchett, RL-83-010, p 37
de Korte P A J, Bleeker J A M, de Boggende A J F, Branduardi-Raymont G, Brinkman A C, Culhane J L, Gronenschild E H B M, Mason I and McKechnie S P 1981a *Space Sci. Rev.* **30** 495
de Korte P A J, Giralt R, Coste J N, Ernu C, Frindel S, Flamand J and Contet J J 1981b *Appl. Opt.* **20** 1080
de Korte P A J and Lainé R 1979 *Appl. Opt.* **18** 236
Dershem E and Schein M 1931 *Phys. Rev.* **37** 1246
Donaldson R R, Patterson S R and Thompson D C 1981 *Proc. SPIE* **316** 32
Ehrenberg W 1949a *J. Opt. Soc. Am.* **39** 741
—— 1949b *J. Opt. Soc. Am.* **39** 746
Elliott S B 1963 *X-ray Optics and X-ray Microanalysis* ed H H Pattee, V E Cosslett and A Engström (New York: Academic) p 215
Elson J M and Bennett J M 1979 *Opt. Engng* **18** 116
Elson J M, Rehn V, Bennett J M, Jones V O and Decker D L 1980 *Proc. 6th Int. Conf. on Vacuum Ultraviolet Radiation Physics, Charlottesville, VA* paper III-43
Ershov O A, Brytov J A and Lukirskii A P 1967 *Opt. Spectrosc.* **22** 66
Feldkamp L A, Stearns M B and Shinozaki S S 1979 *Phys. Rev.* B **20** 1310
Forster R 1928 *Helv. Phys. Acta* **1** 18
Franks A 1981 *Low Energy X-ray Diagnostics. AIP Conf. Proc. 75* ed D T Attwood and B L Henke (New York: AIP) p 179
Giacconi R, Gorenstein P, Murray S S, Schreier E, Seward F, Tananbaum H, Tucker W H and Van Speybroeck L 1981 *Telescopes for the 1980s. Ann. Rev. Monograph* ed G Burbidge and A Hewitt p 195
Giacconi R, Gursky H, Paolini F and Rossi B 1962 *Phys. Rev. Lett.* **9** 439
Giacconi R, Reidy W P, Vaiana G S, Van Speybroeck L P and Zehnpfennig T F 1969 *Space Sci. Rev.* **9** 3
Giacconi R and Rossi B 1960 *J. Geophys. Res.* **65** 773
Giacconi R *et al* 1979 *Astrophys. J.* **230** 540
Gorenstein P 1979 *Proc. SPIE* **184** 63
Hagemann H-J, Gudat W and Kunz C 1974 *DESY Rep.* SR-74/7
Hasinger G 1980 *Diploma Thesis* Universität München
Hendrick R W 1957 *J. Opt. Soc. Am.* **47** 165
Henke B L 1981a *Low Energy X-ray Diagnostics. AIP Conf. Proc. 75* ed D T Attwood and B L Henke (New York: AIP) p 146
—— 1981b *Low Energy X-ray Diagnostics. AIP Conf. Proc. 75* ed D T Attwood and B L Henke (New York: AIP) p 340
Henke B L, Lee P, Tanaka T J, Shimabukuro R L and Fujikawa B K 1982 *Atom. Nucl. Data Tables* **27** 1
Henry J P, Spiller E and Weisskopf M 1981 *Proc. SPIE* **316** 166
Herring J R H 1982 *New Techniques in X-ray and XUV Optics. Proc. RAL Symp.* ed B J Kent and B E Patchett, RL-83-010 p 85
Heynacher E and Reinhardt D 1979 *Proc. SPIE* **184** 167
Hudec R and Valníček B 1984 *Adv. Space Res.* **3** No 10-12, 545
Hunter W R, Michels D J, Fleetwood C N, Mangus J D and Bach B W 1980 *Appl. Opt.* **19** 2128
Ishimaru A 1978 *Wave Propagation and Scattering in Random Media* (New York: Academic)
Jentzsch F 1929 *Phys. Z.* **30** 268

Johnson G L and Wuerker R F 1963 *X-ray Optics and Microanalysis* ed H H Pattee, V E Cosslett and A Engström (New York: Academic) p 229
Kast J W 1975 *Appl. Opt.* **14** 537
Kiessig H 1931 *Ann. Phys., Lpz.* **10** 769
Kirkpatrick P and Baez A V 1948a *Bull. Am. Phys. Soc.* **23** 10
—— 1948b *J. Opt. Soc. Am.* **38** 776
Korsch D 1979 *Opt. Engng* **18** 331
Lainé R, Girault R, Zobl R, de Korte P A J and Bleeker J A M 1979 *Proc. SPIE* **184** 181
Ledger A M 1979 *Proc. SPIE* **184** 176
Lenzen R 1975 *Diploma Thesis* Universität Tübingen
—— 1978 *PhD Thesis* Universität München
Lindsey K 1973 *Proc. X-ray Optics Symp., Mullard Space Science Laboratory, University College London* ed P W Sandford p 101
Lindsey K and Penfold A B 1976 *Opt. Engng* **15** 220
Lukirskii A P, Savinov E P, Ershov O A and Shepelev Yu F 1964 *Opt. Spectrosc.* **16** 168
Malina R F, Bowyer S, Finley D and Cash W 1980 *Opt. Engng* **19** 211
Mandelstam S L, Kurt V G, Valnicek B I, Vainstein L A, Sheffer E K, Slemzin V A and Zhitnik I A 1983 *Adv. Space Res.* **2** No 4 293
Mangus J D 1970 *Appl. Opt.* **9** 1019
Mangus J D and Underwood J H 1969 *Appl. Opt.* **8** 95
Mathur D P, Adamo D R, Bastien R C and Strouse E A 1979 *Proc. SPIE* **184** 139
Névot L and Croce P 1975 *J. Appl. Crystallogr.* **8** 304
—— 1980 *Rev. Phys. Appl.* **15** 761
Pfeffermann E and Briel U 1983 *Adv. Space Res.* **2** No 4, 255
Predehl P, Bräuninger H, Kraus H and Trümper J 1981 *Proc. SPIE* **316** 128
Price R H 1981 *Low Energy X-ray Diagnostics. AIP Conf. Proc. 75* ed D T Attwood and B L Henke (New York: AIP) p 189
Rehn V, Jones V O, Elson J M and Bennett J M 1980 *Nucl. Instrum. Meth.* **172** 307
Röntgen W C 1895 *Sitzungsberichte der Würzburger Physikalischen-Medicinischen Gesellschaft*
Savinov E P, Lyakhowskaya J J, Ershov O A and Kowalyeva E A 1970 *Opt. Spectrosc.* **27** 179
Schlüter M 1972 *Z. Phys.* **250** 87
Schmahl G, Rudolph D and Niemann B 1981 *Proc. SPIE* **316** 100
Schmidt W K H 1975 *Nucl. Instrum. Meth.* **127** 285
Schroeder J B and Klimasewski R G 1968 *Appl. Opt.* **7** 1921
Schwarzschild K 1905 *Abh. Wiss. Göttingen* Bd. IV Nr. 2
Serlemitsos P J 1981 *X-ray Astronomy in the 1980's* ed S S Holt *NASA Tech. Mem.* 83848, p 441
Seward F and Macdonald A 1983 *Einstein (HEAO-2) Observing Catalog* CFA/HEA83-039, 4th edn
Smirnov L A 1980 *Opt. Spectrosc.* **48** 629
Smirnov L A, Sotnikova T D, Anokhin B S and Taibin B Z 1979 *Opt. Spectrosc.* **46** 329
Sommargren G E 1981 *Appl. Opt.* **20** 610
Spiller E 1981 *Low Energy X-ray Diagnostics. AIP Conf. Proc. 75* ed D T Attwood and B L Henke (New York: AIP) p 124
Stedman M 1981 *Proc. SPIE* **316** 2
Stephan K-H, Predehl P, Aschenbach B, Bräuninger H and Ondrusch A 1981 *Proc. SPIE* **316** 203
Stewardson E A and Underwood J H 1965 *Br. J. Appl. Phys.* **16** 1877
Tatchyn R, Lindau I, Källne E, Hecht M, Spiller E, Bartlett R, Källne J, Dijkstra J H, Hawryluk A and Bacharach R Z 1982 *Nucl. Instrum. Meth. Phys. Res.* **195** 423
Taylor B G, Andresen R D, Peacock A and Zobl R 1981 *Space Sci. Rev.* **30** 479
Trümper J 1983 *Adv. Space Res.* **2** No 4, 241
—— 1984 *Phys. Scr.* **T7** 209
Trümper J, Aschenbach B and Bräuninger H 1979 *Proc. SPIE* **184** 2
Ulmer M P, Purcell W R Jr, Loughlin J E A and Kowalski M P 1984 *Electroform Replication used for Multiple X-ray Mirror Production. Preprint* Northwestern University
Underwood J H 1975 *Space Sci. Rev.* **1** 289
Underwood J H, Milligan J E, de Loach A C and Hoover R C 1977 *Appl. Opt.* **16** 858
Underwood J H and Barbee T W 1981 *Nature* **294** 429
Vaiana G S, Van Speybroeck L P, Zombeck M V, Krieger A S, Silk J K and Timothy A F 1977 *Space Sci. Instrum.* **3** 19

Van Speybroeck L P 1973 *Proc. X-ray Optics Symp., Mullard Space Science Laboratory, University College London* ed P W Sandford p 31
—— 1977 *Proc. SPIE* **106** 136
—— 1979 *Proc. SPIE* **184** 2
Van Speybroeck L P and Chase R C 1972 *Appl. Opt.* **11** 440
Van Speybroeck L P, Chase R C and Zehnpfennig T F 1971 *Appl. Opt.* **10** 945
Voglmaier R 1984 *Diploma Thesis* Universität München
Welford W T 1977 *Opt. Quantum Electron.* **9** 269
Werner W 1977 *Appl. Opt.* **16** 764
Williams A C J D, Reily J C, Weisskopf M C, Wyman C L and Zombeck M V 1984 *NASA Tech. Mem.* 82570
Williams A C and Reily J C 1984 *Opt. Engng* **23** 177
Willingale R 1982 *New Techniques in X-ray and XUV Optics. Proc. RAL Symp.* ed B J Kent and B E Patchett, RL-83-010 p 124
Wills-Moren W J 1982 *New Techniques in X-ray and XUV Optics. Proc. RAL Symp.* ed B J Kent and B E Patchett, RL-83-010 p 135
Winkler C E and Korsch D 1977 *Appl. Opt.* **16** 2464
Wolter H 1952a *Ann. Phys., NY* **10** 94
—— 1952b *Ann. Phys., NY* **10** 286
—— 1971 *Opt. Acta* **18** 425
Wriston R S and Froechtenigt J F 1973 *Appl. Opt.* **12** 25
Young P S 1979 *Proc. SPIE* **184** 131
Zombeck M V 1981 *Opt. Engng* **20** 305
—— 1982 *Advanced X-ray Astrophysics Facility (AXAF) Interim Rep.* SAO-AXAF-82-010
—— 1983a *Advanced X-ray Astrophysical Facility (AXAF) Interim Rep.* SAO-AXAF-83-016
—— 1983b *Adv. Space Res.* **2** No 4, 259
—— 1983c *Advanced X-ray Astrophysical Facility (AXAF) Interim Rep.* SAO-AXAF-83-015
Zombeck M V, Bräuninger H, Ondrusch A and Predehl P 1981 *Proc. SPIE* **316** 174
Zombeck M V, Wyman C C and Weisskopf M C 1982 *Opt. Engng* **21** 63